Title

Microglial dyshomeostasis drives perineuronal net and synaptic loss in a CSF1R+/− mouse model of ALSP, which can be rescued via CSF1R inhibitors

Journal

Science Advances, 7(35)

ISSN

2375-2548

Authors

Arreola, Miguel A

Soni, Neelakshi

Crapser, Joshua D

et al.

Publication Date

2021-08-27

DOI

10.1126/sciadv.abg1601

NEUROSCIENCE

Microglial dyshomeostasis drives perineuronal net and synaptic loss in a CSF1R$^{+/-}$ mouse model of ALSP, which can be rescued via CSF1R inhibitors

Miguel A. Arreola[1], Neelakshi Soni[1], Joshua D. Crapser[1], Lindsay A. Hohsfield[1], Monica R. P. Elmore[1], Dina P. Matheos[1], Marcelo A. Wood[1], Vivek Swarup[1], Ali Mortazavi[2], Kim N. Green[1]*

Adult-onset leukoencephalopathy with axonal spheroids and pigmented glia is an autosomal dominant neurodegenerative disease caused by mutations in colony-stimulating factor 1 receptor (CSF1R). We sought to identify the role of microglial CSF1R haploinsufficiency in mediating pathogenesis. Using an inducible *Cx3cr1*$^{CreERT2/+}$-*Csf1r*$^{+/fl}$ system, we found that postdevelopmental, microglia-specific *Csf1r* haploinsufficiency resulted in reduced expression of homeostatic microglial markers. This was associated with loss of presynaptic surrogates and the extracellular matrix (ECM) structure perineuronal nets. Similar phenotypes were observed in constitutive global *Csf1r* haploinsufficient mice and could be reversed/prevented by microglia elimination in adulthood. As microglial elimination is unlikely to be clinically feasible for extended durations, we treated adult CSF1R$^{+/-}$ mice at different disease stages with a microglia-modulating dose of the CSF1R inhibitor PLX5622, which prevented microglial dyshomeostasis along with synaptic- and ECM-related deficits. These data highlight microglial dyshomeostasis as a driver of pathogenesis and show that CSF1R inhibition can mitigate these phenotypes.

INTRODUCTION

Adult-onset leukoencephalopathy with axonal spheroids and pigmented glia (ALSP), also reported as hereditary diffuse leukoencephalopathy with spheroids, is a rare autosomal dominant neurodegenerative white matter disease. Pathologically, this disease is characterized by the presence of patchy cerebral white matter lesions, predominantly in frontal and parietal white matter areas, which induce early thinning of the corpus callosum (cc) followed by subsequent cortical atrophy in the affected regions (*1*–*4*). Genome-wide linkage analyses (GWLAs) have provided a genetic origin of the disease by identifying mutations that affect the tyrosine kinase domain of colony-stimulating factor 1 receptor (CSF1R) in families with ALSP. In the adult brain, CSF1R is primarily expressed by microglia, and mutations found in the GWLAs have been shown to effectively eliminate the kinase activity of this receptor (*5*–*7*). In vitro models demonstrate that autophosphorylation of the tyrosine residues in the kinase domain is impaired in cells with mutated *Csf1r* (*2*, *7*). However, the cellular biology underlying detrimental ALSP phenotypes induced by mutations in *Csf1r* [e.g., cellular source(s) of pathology] remains unclear. Whereas some studies argue for a dominant-negative effect in which expression of the mutant CSF1R suppresses autophosphorylation of the wild-type (WT) CSF1R (*7*, *8*), others argue for a predominantly functional haploinsufficiency genetic mechanism (*9*, *10*). However, the discovery that *Csf1r* haploinsufficiency alone could cause ALSP in the clinical population without requiring the expression of mutated protein (*2*, *11*) leads to the subsequent development of CSF1R$^{+/-}$ mice as a model of disease. This mouse model develops behavioral and histopathological deficits similar to those found in patients with ALSP including depression, seizures, cognitive deficits, abnormal myelination, and neurodegeneration (*12*), highlighting the validity of using these mice to investigate disease-related mechanisms. In addition to *Csf1r*, mutations in other genes highly expressed in microglia (*Trem2* and *Tyrobp*) are known to cause progressive leukodystrophies and neurodegenerative disorders aside from ALSP, broadly termed microgliopathies (*13*, *14*).

As central nervous system (CNS)–resident macrophages, microglia modulate CNS homeostasis by orchestrating inflammatory responses (*15*), clearing cellular debris (*16*, *17*), restructuring synapses (*18*, *19*), and regulating perineuronal nets (PNNs) (*19*–*21*). Understanding how changes in microglial function that result from *Csf1r* haploinsufficiency, or other factors, can affect these various modalities may inform us about how microglia cause neurodegeneration in related microgliopathies. This information can be extended to understand how altered microglial functions can affect CNS stability and contribute to neurodegeneration in other disorders such as Alzheimer's disease (AD), Parkinson's disease, tauopathies, stroke, and injury, as well as aging itself. Whether microglial gain of function or loss of function results in ALSP phenotypes, however, is still up for debate. In addition, expression of CSF1R in neurons during development has been noted in mice (*22*, *23*), and thus, it is critical to delineate microglial versus nonmicroglial as well as the developmental versus nondevelopmental contributions to disease. Selective knockout of *Csf1r* from neurons using a nestin-cre system in mice resulted in increased cellular apoptosis in the forebrain, as well as an increased pool of neural progenitor cells, despite normal cortical microglial number, suggesting that CSF1R signaling is important for neuronal development and survival (*23*). Of relevance, microglia are dependent on CSF1R signaling for their survival, and sustained pharmacological inhibition of CSF1R, or absence of *Csf1r* expression (*24*), results in microglial death (*25*). Hence, it has been postulated that ALSP could result from loss of homeostatic microglial numbers due to a decreased amount of CSF1R expression during the aging process, as has been shown in a *Csf1r* genetic knockout zebrafish model

[1]Department of Neurobiology and Behavior, University of California, Irvine, Irvine, CA 92697, USA. [2]Department of Developmental and Cell Biology, University of California, Irvine, Irvine, CA 92697, USA.
*Corresponding author. Email: kngreen@uci.edu

(*26*). However, long-term CSF1R inhibitor–dependent microglial elimination in mice (up to 6 months of treatment) does not cause any overt impairments as related to ALSP and improves cognition in some cases, as assessed by contextual fear conditioning, Morris water maze, Barnes maze, and elevated plus maze (EPM) (*25*, *27*). Nonetheless, given the primary role of CSF1R in both microglial survival and ALSP and of the frequent microglial gene–specific etiology of leukodystrophies in general, it is likely that pathological alterations in microglial function contribute to ALSP onset and/or progression.

In the present study, we aimed to investigate how loss of one *Csf1r* allele would affect microglial and parenchymal homeostasis. Here, we found that myeloid-specific ablation of one copy of the *Csf1r* gene in adult mice resulted in a general loss of microglial homeostasis as evident by loss of P2RY12 (Purinergic Receptor P2Y12) expression. Accompanying this microglial dyshomeostasis, we observed a decrease in synaptic surrogates, as well as dysregulation of extracellular matrix (ECM) components, in particular, a loss of PNNs, confirming an adult microglial origin for these downstream phenotypes. Using a constitutive CSF1R$^{+/-}$ mouse model of ALSP, we noted an increase in microglia densities, due to developmental defects in the establishment of the adult microglial population, and a similar loss of P2RY12 expression and microglial hyper-ramification in CSF1R$^{+/-}$ mice. Accompanying this loss in microglial homeostasis, we observed impaired behavioral output assessed by novel object recognition (NOR) and novel place recognition (NPR) tasks, along with similar decreases in synaptic surrogates and PNNs. Accordingly, complete elimination of microglia from adult CSF1R$^{+/-}$ mice reverses PNN and synaptic deficits. We further compared the genetic monoallelic loss of *Csf1r* with low-grade chronic CSF1R inhibition and found substantial overlap in gene expression changes, suggesting that partial disruptions to CSF1R signaling, whether pharmacological or genetic in nature, lead to similar downstream signaling abnormalities. Unexpectedly, low-grade CSF1R inhibition in CSF1R$^{+/-}$ mice was able to reverse microglial dyshomeostasis and restore cognition, as well as prevent the loss of synaptic surrogates and PNNs in affected mice, rather than exacerbate these alterations. Further, analysis of aged CSF1R$^{+/-}$ mice revealed marked loss of myelin basic protein (MBP) staining in the cc and ECM structures in the somatosensory cortex (SS Ctx), of which PNNs were rescued when treated with low-grade CSF1R inhibition. These data indicate that CSF1R signaling is key to maintaining microglial homeostasis, specifically regulating the effects of microglia on both synapses and the ECM in which synaptic connections are embedded, and may be targeted to both perturb and rescue microglial phenotype.

RESULTS

Microglia-specific monoallelic *Csf1r* knockout in adult mice induces loss of presynaptic markers, disruption to the ECM compartment, and microglial dyshomeostasis

While CSF1R is exclusively expressed in microglia in the adult brain (*28*), expression of this receptor has also been reported in specific neuronal populations during brain development (*23*, *29*). As CSF1R$^{+/-}$ mice lack one *Csf1r* allele in all cells throughout their life span, we sought to fully establish the microglial and adult origin of any disruptions induced by *Csf1r* haploinsufficiency that may be relevant to ALSP pathogenesis. To this end, we crossed *Cx3cr1*-Cre$^{ERT2/+}$ mice with floxed *Csf1r*$^{+/fl}$ mice to generate mice in which we could inducibly and specifically ablate a *Csf1r* allele from adult microglia. Progeny from this pairing resulted in two groups: CX3CR1^{Cre}-CSF1R$^{+/+}$ (Con) and CX3CR1^{Cre}-CSF1R$^{+/fl}$ (iCSF1R$^{+/-}$) mice. At 2 months of age (i.e., in adult mice), we administered tamoxifen to selectively excise a single CSF1R allele from microglia/myeloid cells, and animals were subsequently sacrificed at 8 months old (Fig. 1A). Because events leading up to overt CNS pathology in ALSP are still poorly understood, we chose to focus our study on a time point at which cognitive deficits are detectable, but white matter and axonal damage is not yet apparent, based on published data from global *Csf1r* haploinsufficient mice (*12*). To confirm the efficient recombination and knockdown of *Csf1r* expression, we quantified *Csf1r* mRNA via RNAscope in situ hybridization and found 40 to 50% reduced levels of *Csf1r* RNA in iCSF1R$^{+/-}$ mice compared to Con mice (Fig. 1, B and C). Notably, *Csf1r* mRNA was absent in neurons at this time point. Because *Csf1r* is a primarily microglia-expressed gene in the adult brain and studies of postmortem ALSP brains report microglial dysregulation preceding axonal pathology (*3*) further suggesting microglial involvement during early disease onset, we first analyzed cortical microglial densities. Despite apparent *Csf1r* down-regulation, cortical microglial numbers were unaffected in iCSF1R$^{+/-}$ animals (Fig. 1, D and E), in contrast to the reported ~25% elevation in microglial densities reported in global *Csf1r* haploinsufficient mice (*12*, *30*), and no overt morphological signs of microglial reactivity were seen (i.e., deramified enlarged cell bodies and retracted and condensed processes). Because *Csf1r* can be expressed by perivascular macrophages (PVMs), we immunostained for these with antibodies against CD206 and found no changes to the number of PVMs between Con and iCSF1R$^{+/-}$ groups (fig. S1, A and B).

Under homeostatic conditions, the microglial transcriptome is characterized by the expression of genes such as *Sall1*, *Hexb*, *Cx3cr1*, *Tmem119*, *Trem2*, *P2ry12*, *Mertk*, and *SiglecH* (*30*, *31*). While these genes are uniquely and highly expressed by microglia during homeostasis, under states of duress or neurodegeneration, this subset of genes is down-regulated (*31*–*33*). This down-regulation, however, is transient in some cases—during periods of recovery, microglia have been observed to up-regulate these same genes (*32*). A recent study noted reduced expression of P2RY12 in patients with ALSP (*34*); hence, we stained for P2RY12 to examine the homeostatic status of microglia and observed reduced microglial expression of this marker in iCSF1R$^{+/-}$ mice (Fig. 1, F and G). Similarly, we observed reduced expression of the homeostatic marker (Transmembrane Protein 119) in iCSF1R$^{+/-}$ mice (fig. S2, A and B).

Previous studies have shown that dysfunctional microglia are active participants in the structural and functional alteration of synapses that culminates in synaptic impairment and degradation (*35*, *36*). Therefore, we investigated cortical synaptic integrity by quantifying known pre- and postsynaptic markers (*37*–*39*). iCSF1R$^{+/-}$ mice showed significant reductions in presynaptic markers (Synaptophysin, SV2A, and Bassoon; Fig. 1, H to M; Fig. 1H′, example Imaris-quantified puncta) but no changes in the postsynaptic marker PSD95 (Postsynaptic density protein 95) (Fig. 1, N and O).Within the framework of the tetrapartite synapse model (*40*), the ECM has emerged as a vital component involved in the modulation of synaptic plasticity (*41*, *42*), stabilization of synaptic contacts (*42*, *43*), and overall learning and memory (*41*, *42*). Recently, we demonstrated that microglia in mouse models of Huntington's disease (HD) and AD induced profound changes in the ECM, including notable reductions in specialized interneuron-associated structures known as PNNs that occurred

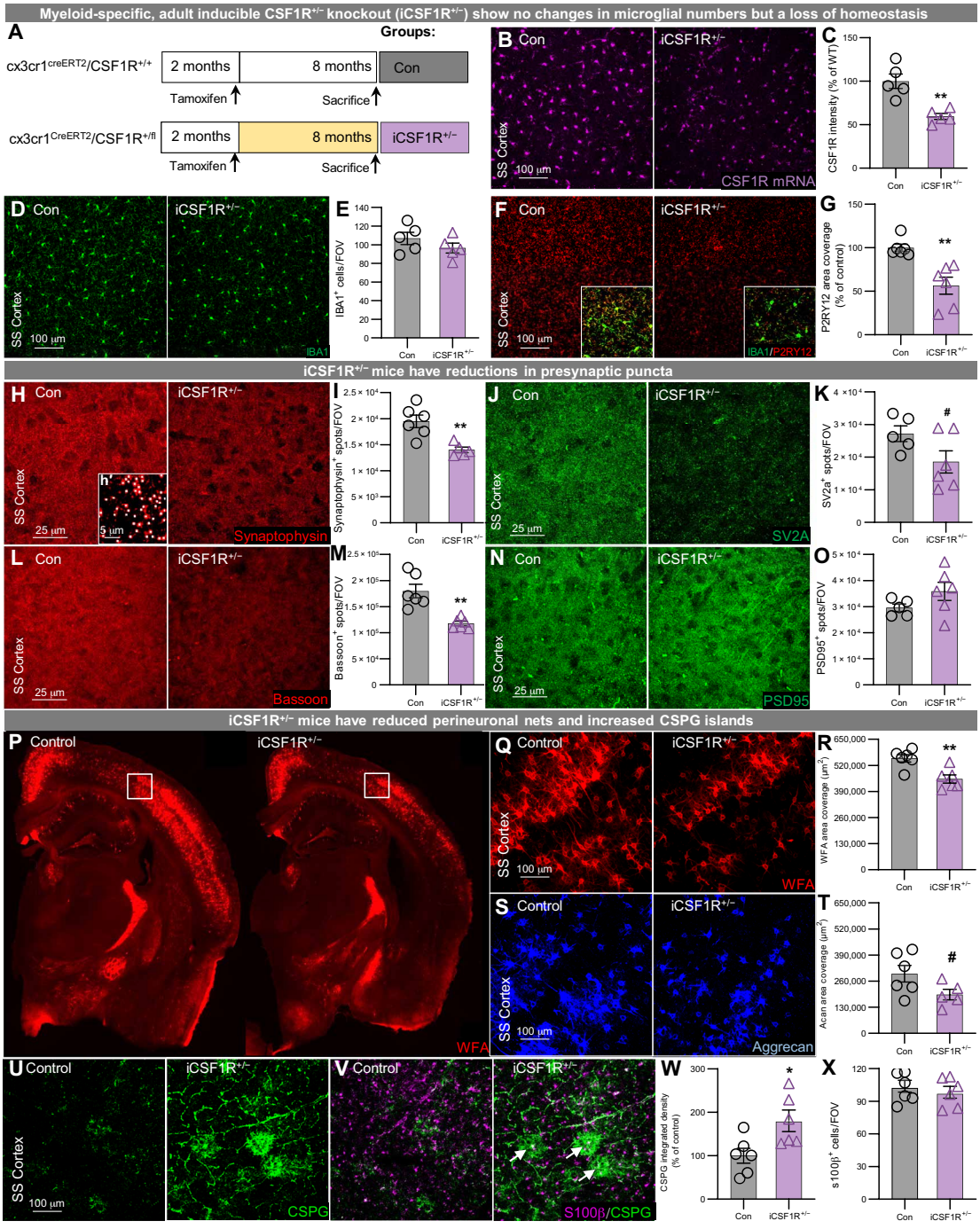

Fig. 1. Myeloid-specific CSF1R$^{+/-}$ (iCSF1R) in adult mice confirms loss in homeostasis, reductions in synaptic surrogates, and alterations in ECM structures. (**A**) Experimental paradigm whereby tamoxifen was introduced via oral gavage to cx3cr1^{cre}-CSF1R$^{+/fl}$ and cx3cr1^{cre}-CSF1R$^{+/+}$ mice at 2 months, well after microglial development. Mice were sacrificed at 8 months. (**B** and **C**) Representative image of 20× in situ hybridization of CSF1R RNA reveals a 40 to 50% reduction in CSF1R expression throughout. (**D** and **E**) Representative 20× image of IBA1$^+$ immunofluorescence in the SS Cortex revealed no significant changes to IBA1$^+$ cell number. (**F** and **G**) Representative 20× image of SS Cortex revealed significant decrease in P2RY12 expression by microglia. Insets display Iba1 P2ry12 immunostaining. Myeloid-specific CSF1R knockout mice presented with losses of presynaptic puncta (**H** and **I**) Synaptophysin, (**J** and **K**) SV2A, and (**L** and **M**) Bassoon. (H') Example Imaris quantification of Synaptophysin$^+$ spots digitally zoomed in 5× from 63× image. (**N** and **O**) No differences found in PSD95 puncta number, however. (**P**) Whole-brain stitches of half brains of myeloid-specific CSF1R haploinsufficient mice immunostained for WFA. (**Q** and **R**) Representative 20× images of WFA and aggrecan immunostaining in SS Cortex, respectively. (**S** and **T**) Quantification confirmed significant decrease in WFA and aggrecan (Acan) area coverage found in global CSF1R$^{+/-}$ haploinsufficient mice. (**U** and **V**) Representative 20× confocal images of SS Cortex immunostained for CSPG and S100β$^+$ (**W**) display a significant increase in CSPG accumulation as measured by integrated density (**X**) and no changes in S100β$^+$ cells. Statistical analysis for inducible CSF1R$^{+/-}$ comparisons used a two-tailed *t* test. Significance is indicated as *$P < 0.05$; **$P < 0.01$; #$0.05 < P < 0.1$. FOV, field of view; WFA, *W. floribunda* agglutinin.

concomitant with the accumulation of chondroitin sulfate proteoglycans (CSPGs) in the general ECM (*20*, *44*). iCSF1R$^{+/-}$ mice show robust reductions in SS Ctx PNNs, via stains for both *W. floribunda* agglutinin (WFA), a plant lectin commonly used to label PNNs, and aggrecan, a CSPG selectively expressed by PNNs necessary for their construction and maintenance (*46*) (Fig. 1, P to T), indicating that loss of a single *Csf1r* allele in adult microglia is sufficient to induce PNN degradation and/or loss.

We next explored the presence of CSPGs with chondroitin-6 sulfate patterns via the CS-56 antibody (*46*). While aggrecan is primarily found in PNNs, CS-56^{+} staining presents as "dandelion clocklike structures" (DACS) distinct from PNNs (*47*). In ketamine models of schizophrenia, the prefrontal cortex exhibits reduced levels of PNNs and increased intensity of DACS staining (*48*), similar in pattern to what we reported in HD, wherein elimination of microglia rescued the increased accumulation of DACS (*20*). Here, we find that iCSF1R$^{+/-}$ mice show markedly increased CS-56^{+} staining throughout the brain (Fig. 1, U and W). While these CSPG structures are primarily produced by astrocytes (*49*), and we often observed astrocytes at the center of these deposits (Fig. 1V, arrows), it should be noted that we did not detect any changes to astrocyte density as assessed by S100β^{+} cell number across groups (Fig. 1X). It has been reported that CS-56^{+} up-regulation occurs around reactive astrocytes in physical proximity to activated microglia/macrophages (*50*). Crucially, these results show that loss of one *Csf1r* allele from adult *Cx3cr1*-expressing resident myeloid cells (i.e., microglia) is sufficient to induce disturbances in microglial homeostasis as reflected in the loss of P2RY12 immunofluorescence, presynaptic dysfunction, and dysregulation of the ECM.

Microglial depletion reverses presynaptic and ECM alterations induced by *Csf1r* haploinsufficiency

Our results show that microglial loss of a *Csf1r* allele in adult mice leads to cellular dyshomeostasis, concomitant with a loss of presynaptic puncta and remodeling of the ECM. To further confirm the microglial origin of these CSF1R-associated phenotypes, to complement with a more clinically relevant model of ALSP, and to determine the extent to which pathology can be rescued, we next sought to eliminate virtually all microglia from adult CSF1R$^{+/-}$ mice (i.e., global CSF1R haploinsufficiency), which can be achieved by administration of the CSF1R inhibitor PLX5622 [1200 parts per million (ppm) in chow] (*27*). WT and CSF1R$^{+/-}$ mice were treated for 2 months beginning at 6 months (Fig. 2A) to align with the 8-month-old iCSF1R$^{+/-}$ mice. This paradigm generated four groups: WT and CSF1R$^{+/-}$ groups as well as their microglia-depleted (MD) counterparts MD-WT and MD-CSF1R$^{+/-}$. Quantification of IBA1^{+} (ionized calcium binding adaptor molecule 1) cells confirmed depletion of >90% of microglia in MD-WT and MD-CSF1R$^{+/-}$ mice [interaction: $F(1,15) = 21.88$, $P = 0.0003$; post hoc significance between groups displayed on graph; Fig. 2, B and C], with CSF1R$^{+/-}$ mice showing elevated densities of microglia compared to WT mice, in accordance with prior studies (*12*, *51*). This is in contrast to what we observed in adult microglia-specific *Csf1r* haploinsufficient mice (iCSF1R$^{+/-}$ mice; Fig. 1D), suggesting that elevated microglial densities may be established during development (e.g., before tamoxifen-induced *Csf1r* excision), further explored in our developmental time course experiment (Fig. 4). Despite this, and in accordance with iCSF1R$^{+/-}$ mice, Synaptophysin^{+}, SV2a^{+}, and Bassoon^{+} puncta were all significantly reduced in CSF1R$^{+/-}$ mice (Fig. 2, D to I). Elimination of microglia in CSF1R$^{+/-}$ mice increased synaptic puncta density for all markers [interaction: $F(1,18) = 3.924$ $P = 0.06$; $F(1,19) = 9.058$ $P = 0.0072$; and $F(1,18) = 8.738$ $P = 0.0085$ for Synaptophysin, SV2a, and Bassoon, respectively, significance between groups displayed on graph]. In addition, CSF1R$^{+/-}$ mice displayed a marked reduction in PNNs as assessed by WFA and aggrecan immunostaining, which are also restored upon microglial elimination [interaction: $F(1,19) = 3.380$ $P = 0.08$ and $F(1,19) = 3.727$ $P = 0.06$ for WFA and aggrecan, respectively, significance between groups displayed on graph; Fig. 2, J to M]. Last, similar disease-associated CS-56^{+} CSPG up-regulation was evident in the CSF1R$^{+/-}$ brain as in iCSF1R$^{+/-}$ and was reduced with microglial depletion [interaction: $F(1,20) = 57.751$ $P = 0.02$ significance between groups displayed on graph; Fig. 2, N and O]. These data further suggest a disease phenotype primarily driven by malfunctioning microglia and the downstream detrimental effects that they exert on neuronal populations, which, importantly, may be mitigated by pharmacological targeting of the former, at least in early stages of disease.

CSF1R$^{+/-}$ mice display cognitive deficits that are rescued by sustained low-grade CSF1R inhibition

The elimination of the microglial compartment for extended periods of time via CSF1R inhibitors is unlikely to be clinically feasible in patients with ALSP; therefore, we sought to identify potential treatments that could mitigate disease by modulating, rather than removing, the microglial phenotype. Notably, lower doses of CSF1R inhibitors that do not eliminate the microglial compartment have been shown to nonetheless alter disease-related microglial phenotypes and provide protection in animal models of AD (*52*, *53*), Prion disease (*54*), and tauopathies (*55*). To that end, we developed a CSF1Ri regimen that led to reduced effects of CSF1R inhibition such that there was modest microglial death compared to higher dosages, which eliminate more than 95% of microglia (fig. S3A). WT and CSF1R$^{+/-}$ mice were treated with the specific CSF1R inhibitor PLX5622 (150 ppm in chow) for 2 months starting at 6 months to induce CSF1Ri. Thus, four groups were generated: WT, CSF1Ri, CSF1R$^{+/-}$, and CSF1Ri-CSF1R$^{+/-}$ (Fig. 3A). This dosage of PLX5622 was determined in a separate subset of mice to provide microglial CSF1R inhibition that eliminates <25% of microglia under either homeostatic or inflammatory conditions (fig. S3, B and C). Quantitative polymerase chain reaction (PCR) confirmed half the level of *Csf1r* transcripts in CSF1R$^{+/-}$ mice compared to WT mice (Fig. 3B).

ALSP is characterized by executive dysfunction, memory decline, motor impairments, and a lack of social inhibitions. In studies characterizing phenotypes of *Csf1r* haploinsufficient mice, cognitive deficits are reported to begin at 7 months (*12*) that resemble the clinical presentation of ALSP (*4*, *7*), but overt white matter damage is not observed until 14 months. To characterize behavioral phenotypes in our cohort of mice ($n = 8$ to 10), we performed a battery of tasks consisting of EPM, open field (OF), NOR, and NPR. Given the motor impairments, including gait dysfunction, and social withdrawal noted in patients with ALSP, we also included a rotarod and social interaction task. Behavioral assessments began 6 weeks after mice were placed on diet and continued for 2 weeks, at which point mice were euthanized. While we found no significant changes in mobility or anxiety measures in any group as determined by performance in EPM, OF, and social interaction and rotarod tasks (fig. S4, A to F), we observed impairments in cognitive domains as measured by NOR and NPR tasks in CSF1R$^{+/-}$ mice (Fig. 3, C and D).

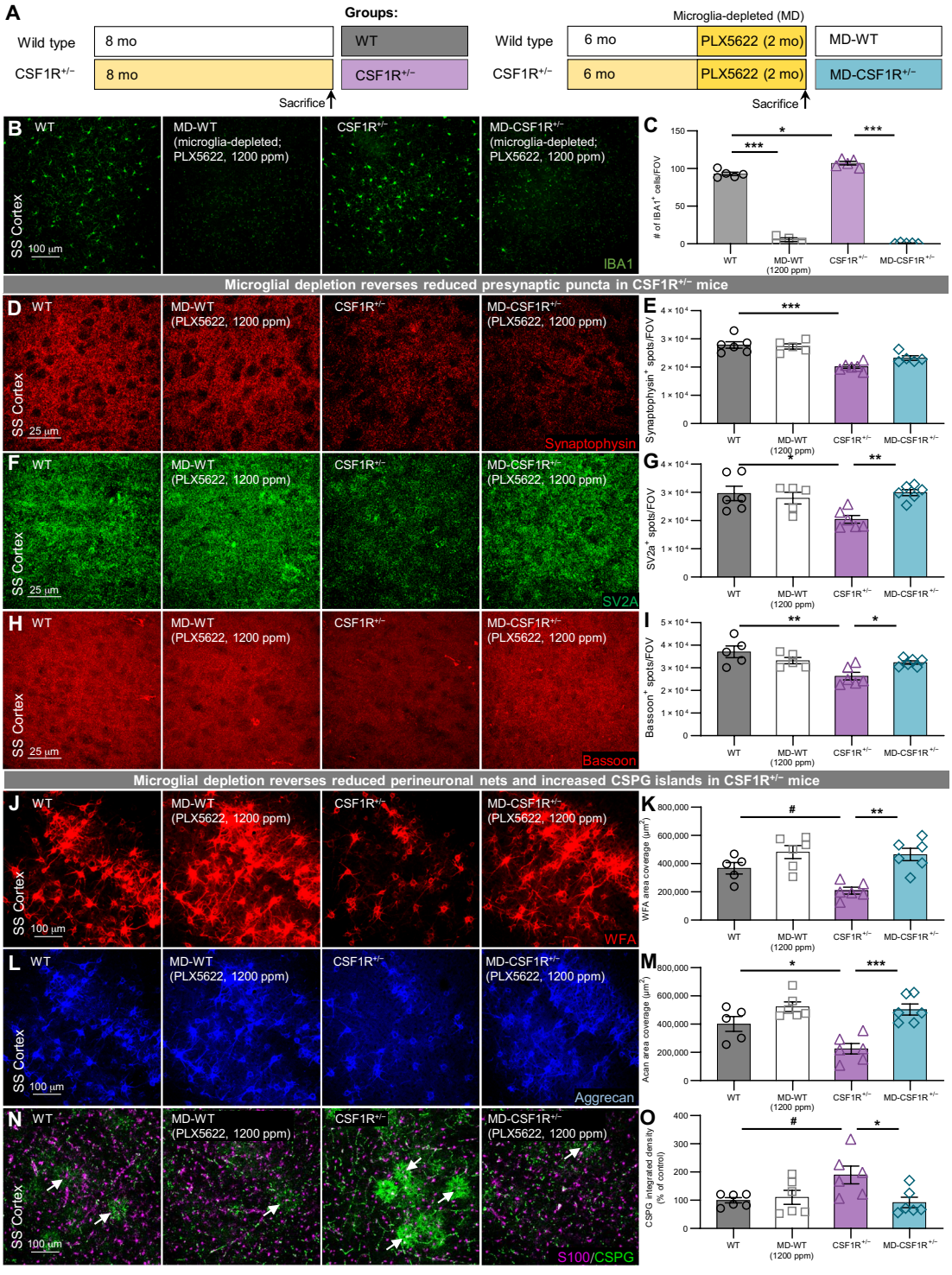

Fig. 2. Elimination of microglia with 1200 ppm of PLX5622 restored synaptic and ECM alterations induced by CSF1R haploinsufficiency. (**A**) WT and CSF1R$^{+/-}$ mice were placed on a high-dose PLX5622 diet (1200 ppm) for 2 months beginning at 6 months to completely eliminate microglia from the brain parenchyma. (**B**) Immunofluorescent image of IBA1^{+} cells in the SS Cortex, (**C**) quantification of which showed significant decrease (~90 to 95% elimination) of microglia in WT and CSF1R$^{+/-}$-treated mice. (**D**, **F**, and **H**) Representative 63× immunofluorescent images of presynaptic elements Synaptophysin, SV2A, and Bassoon, respectively. (**E**, **G**, and **I**) Quantification of these showed significant decreases in the number of puncta in CSF1R$^{+/-}$ SS Cortex and recovery of puncta number in CSF1R$^{+/-}$ mice in which microglia were completely eliminated, with the exception of Synaptophysin. (**J** to **M**) Immunostaining of WFA and aggrecan displayed decreased PNN area coverage in SS Cortex of CSF1R$^{+/-}$ mice. Elimination of microglia restored ECM composition in CSF1R$^{+/-}$ mice. (**N** and **O**) Immunostaining and quantification of *CSPG* revealed increased immunostaining of CS-56 in CSF1R$^{+/-}$ parenchyma that was restored by elimination of microglia. Statistical analysis used a two-way ANOVA with Sidak multiple comparisons correction. Significance is indicated as $^{*}P < 0.05$; $^{**}P < 0.01$; $^{***}P < 0.001$; #$0.05 < P < 0.1$.

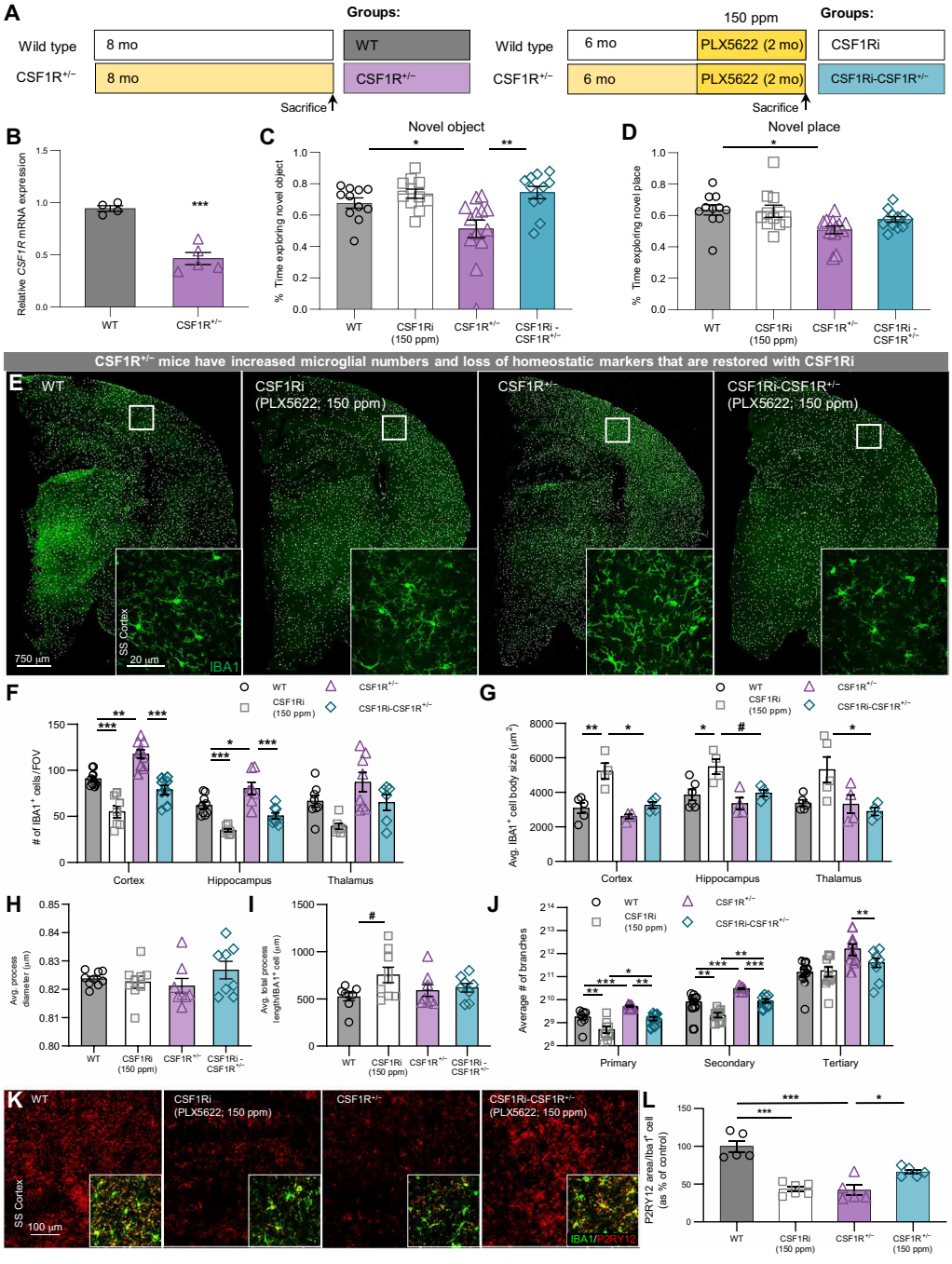

Fig. 3. CSF1R$^{+/-}$ mice display behavioral and morphological deviations from WT counterparts that are restored by CSF1Ri. (**A**) WT and CSF1R$^{+/-}$ mice were treated with 150 ppm of PLX5622 for 2 months beginning at 6 months. Mice were sacrificed at 8 months ($n = 8$ to 10 per group). (**B**) Relative expression levels of CSF1R normalized to glyceraldehyde-3-phosphate dehydrogenase via quantitative PCR. Expression levels of CSF1R in CSF1R$^{+/-}$ were reduced ~50% compared to WT ($P < 0.0001$) using two-tailed t test. (**C**) CSF1R$^{+/-}$ mice spent significantly less time exploring the novel object compared to WT mice. CSF1Ri rescued performance comparable to WT counterparts. (**D**) CSF1R$^{+/-}$ mice spent significantly less time exploring objects moved to a novel place compared to WT mice. (**E**) Representative half-brain stitches; each white dot represents a microglial cell. Representative 63× image of SS Cortex IBA1 immunofluorescence. (**F**) Quantification of IBA1$^+$ cells in cortex, hippocampus, and thalamus shows 25 to 30% increase in IBA1$^+$ cells. CSF1Ri treatment reduced IBA1$^+$ cells by 25% in both WT and CSF1R$^{+/-}$ mice. (**G**) Average soma size of IBA1$^+$ cells reveals significantly increased soma size in CSF1Ri microglia. WT IBA1$^+$ cells had comparable soma size to CSF1R$^{+/-}$ and CSF1Ri-CSF1R$^{+/-}$. (**H**) No changes to average process diameter or (**I**) average total process length were found between groups; a trending increase in CSF1Ri microglia was found between WT and CSF1Ri. (**J**) Analysis of branch patterns revealed decreased number of primary and secondary branches in CSF1Ri microglia compared to WT. CSF1R$^{+/-}$ microglia had increased numbers of primary, secondary, and tertiary branching that were reduced to WT levels by CSF1Ri. (**K** and **L**) Representative 20× image of the SS Cortex reveals decreased P2RY12 immunopositivity in CSF1Ri and CSF1R$^{+/-}$ mice. CSF1Ri-CSF1R$^{+/-}$ mice revealed increased expression in P2RY12 expression. Insets display Iba1$^+$ P2RY12$^+$ immunostaining. Statistical analysis used a two-way ANOVA with Sidak multiple comparisons correction. Significance: *$P < 0.05$; **$P < 0.01$; ***$P < 0.001$; #$0.05 < P < 0.1$.

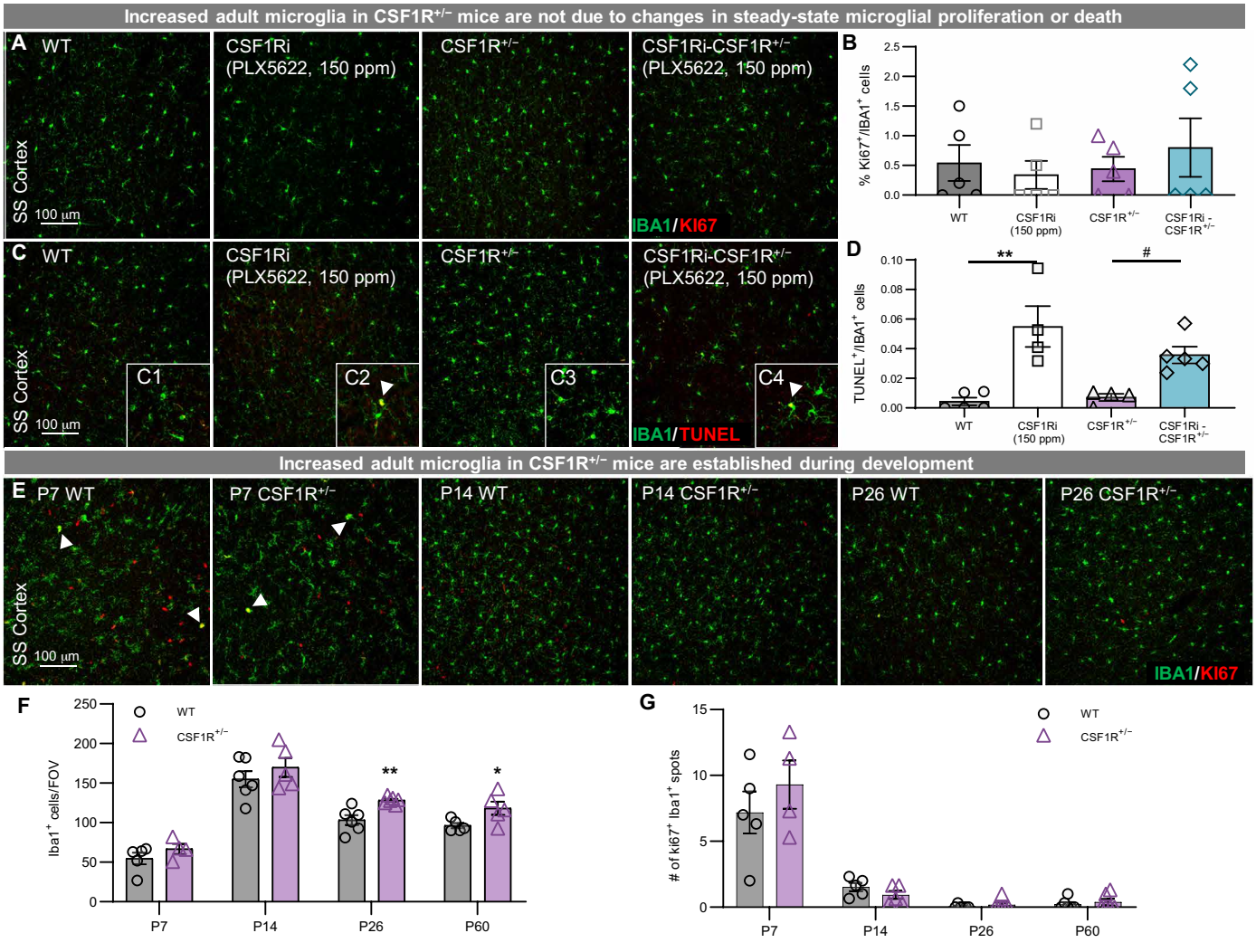

Fig. 4. Increased microglial population is established during development; microglial-specific excision of one CSF1R reveals decreases in microglial molecular markers and dysfunction of a presynaptic marker. (**A**) Representative 20× image of the SS Cortex immunostaining for Ki67 and IBA1$^+$ cells revealed (**B**) no changes to proliferation in any group when compared to WT mice, suggesting that proliferation in the adult cannot account for increased number of IBA1$^+$ cells found in 8-month-old CSF1R$^{+/-}$ mice. (**C**) Representative 20× image of SS Cortex immunostaining for TUNEL and IBA1 revealed that (**D**) CSF1Ri induced an increase in TUNEL IBA1 double-positive cells. (C1 to C4) Arrowheads indicate the presence of TUNEL$^+$/IBA1$^+$ cells. (**E**) Representative 20× images of the SS Cortex of WT and CSF1R$^{+/-}$ mice at P7, P14, and P26 arrows indicate the location of Ki67 IBA1 double positive cells. Immunostaining for IBA1 and Ki67 showed (**F**) no changes in microglial number between WT and CSF1R$^{+/-}$ mice at P7 or P14 but a significant increase in CSF1R$^{+/-}$ at P26 and P60. (**G**) No changes in Ki67 IBA1 double-positive cells were found throughout the time course. Statistical analysis used a two-way ANOVA with Sidak multiple comparisons correction or two-tailed *t* test for developmental study. Significance is indicated as $*P < 0.05$; $**P < 0.01$; $\#0.05 < P < 0.1$.

However, no impairments were evident in CSF1Ri mice by any of these measures [interaction: $F(1,42) = 4.126$ $P = 0.06$ and $F(1,42) = 1.688$ $P = 0.2$ for NOR and NPR tasks, respectively, significance between groups displayed on graph]. These results show that life-long loss of a *Csf1r* allele induces cognitive deficits detectable by 8 months in mice and that such deficits are not similarly evident following sustained (at least 2 months) low-grade CSF1Ri in the healthy adult. Unexpectedly, however, CSF1Ri did rescue cognitive deficits in CSF1R$^{+/-}$ mice in the NOR task (Fig. 3C), revealing that altered CSF1R signaling can induce, and be targeted to rescue, cognitive impairments.

CSF1Ri restores CSF1R$^{+/-}$ microglia number, morphology, and homeostatic marker expression

To better understand the role of CSF1R signaling in cognition, we performed immunohistochemical analyses of myeloid cell attributes in the brain. Here, we found robust increases (~25%) in cortical and hippocampal microglia in CSF1R$^{+/-}$ mice, as shown via immunostaining with antibodies against IBA1 (Fig. 3, E and F), consistent with previous data (*12*). Notably, CSF1Ri treatment of CSF1R$^{+/-}$ mice normalized microglial densities to WT numbers (Fig. 3, E and F). In addition, IBA1$^+$ cell quantification showed a consistent ~25% reduction in microglia following CSF1Ri in both CSF1R$^{+/-}$ and WT

mice, as CSF1Ri-treated CSF1R$^{+/-}$ mice exhibit the same ~25% decrease in IBA1^{+} cell number as CSF1Ri-treated WT animals relative to their respective controls (Fig. 3F), revealing that despite partial loss of CSF1R signaling in CSF1R$^{+/-}$ mice, microglia remain dependent on this signaling pathway for survival. Again, given the expression of *Csf1r* by PVMs, we explored PVM cell populations in our cohorts of mice. Immunostaining of CD206 revealed similar number of PVMs between WT and CSF1R$^{+/-}$ mice and an expected reduction in CSF1Ri-treated groups [interaction: $F(1,17) = 0.0019$ $P = 0.9$ significance between groups displayed on graph; fig. S1, C and D].

Microglial reactivity is a highly dynamic process encompassing a spectrum of phenotypic changes, and under conditions of activation, these changes include an increase in cell size and a loss of process ramification (e.g., amoeboid microglia) (*56*). We found no changes in cell soma size between microglia in WT and CSF1R$^{+/-}$ mice, whereas CSF1Ri in WT, but not CSF1R$^{+/-}$, mice induced significant increases in this measure [interaction: $F(1,13) = 6.095$ $P = 0.02$; $F(1,14) = 0.9976$ $P = 0.33$; $F(1,14) = 5.573$ $P = 0.03$ for cortex, hippocampus, and thalamus, respectively, significance between groups displayed on graph; Fig. 3G]. Analysis of microglial process diameter and average process length revealed no differences between groups [interaction: $F(1,30) = 2.232$ $P = 0.14$ and $F(1,29) = 2.645$ $P = 0.11$ for diameter and process length, respectively, significance between groups displayed on graph; Fig. 3, H and I]. On the other hand, measures of microglial ramification (i.e., primary, secondary, and tertiary branching of microglia processes) showed that CSF1R$^{+/-}$ microglia adopt a hyper-ramified state compared to WT microglia, while CSF1Ri reduced ramification in both WT and CSF1R$^{+/-}$ groups [interaction: $F(1,30) = 0.8740$ $P = 0.35$; $F(1,29) = 0.8646$ $P = 0.36$; and $F(1,30) = 3.117$ $P = 0.08$ for primary, secondary, and tertiary branching, respectively, significance between groups displayed on graph; Fig. 3J]. Examination of microglial P2RY12 revealed decreases in both CSF1Ri and CSF1R$^{+/-}$ microglia (Fig. 3, K and L), as in iCSF1R$^{+/-}$ microglia (Fig. 1, F and G). Rather than further reducing expression, CSF1Ri increased microglial P2RY12 in CSF1R$^{+/-}$ mice [interaction: $F(1,17) = 55.87$ $P = 0.0001$ significance between groups displayed on graph]. This same pattern was observed with TMEM119 expression [interaction: $F(1,18) = 54.59$ $P = 0.0001$ significance between groups displayed on graph; fig. S2, C and D]. Together, these data illustrate the deviation of CSF1R$^{+/-}$ microglia from homeostasis, although more subtle than activation, and suggest that certain biophysical properties of microglia in ALSP (e.g., process ramification and elevated population densities) may be amenable to CSF1Ri treatment, in turn potentially contributing to the rescue of cognitive deficits in CSF1Ri-CSF1R$^{+/-}$ mice.

Increased microglial density is established during early postnatal development

Given the discrepancy between global *Csf1r* haploinsufficiency and adult microglia-specific *Csf1r* haploinsufficiency, whereby only the former results in increases in adult microglial densities, we next explored steady-state turnover of microglia in both adult and developing CSF1R$^{+/-}$ mice. Analysis of adult *CSF1R*$^{+/-}$ mice revealed no changes in either proliferation (via Ki67 staining; Fig. 4, A and B) or apoptosis [via TUNEL (terminal deoxynucleotidyl transferase–mediated deoxyuridine triphosphate nick end labeling); Fig. 4, C and D] of microglia compared to WT, suggesting that steady-state microglial turnover in the adult CSF1R$^{+/-}$ mouse brain parallels that of adult WT microglia. As expected, CSF1Ri treatment in both WT and CSF1R$^{+/-}$ mice increased the number of TUNEL^{+} microglia (Fig. 4, C and D), confirming that CSF1Ri acts by inducing microglia death (*25*). As one copy of *Csf1r* is absent throughout development in *CSF1R*$^{+/-}$ mice and as adult microglial turnover remained similar between WT and CSF1R$^{+/-}$ mice, we next explored the establishment of CSF1R$^{+/-}$ microglial densities during brain development. Early microglia proliferate extensively during the first two postnatal weeks, reaching maximal numbers at postnatal day 14 (P14) (*57*), whereafter this rapid proliferation is followed by a period of selective microglial die-off to establish the final densities of adult microglia by ~P28 (*57*). Quantification of microglia in developing CSF1R$^{+/-}$ mice revealed similar increases in microglial densities due to proliferation between P7 and 14 as seen in WT mice, but this proliferation was followed by decreased reductions in the CSF1R$^{+/-}$ microglial population by P26 (Fig. 4, E to G). This occurred despite equivalent Ki67^{+} proliferation at all developmental time points measured, suggesting that elevated microglial densities in adult CSF1R$^{+/-}$ mice could be due to developmental defects in the establishment of the adult microglial compartment (e.g., impaired microglial die-off). These data are in line with recent evidence wherein constitutive microglial *Csf1r* haploinsufficiency resulted in increased microglial density (*58*), consistent with the lack of differences that we observed in iCSF1R$^{+/-}$ mice, in which monoallelic knockdown of microglial *Csf1r* was induced only after development.

CSF1Ri restores CSF1R$^{+/-}$ synaptic and ECM deficits without changes to neuronal populations

Confirming the synaptic deficits in the prior cohort of CSF1R$^{+/-}$ and iCSF1R$^{+/-}$ mice, we found that CSF1R$^{+/-}$ mice again displayed significant reductions in presynaptic markers (i.e., Synaptophysin, SV2A, and Bassoon) but not the postsynaptic marker PSD95 (Fig. 5, A to H). Treatment of WT mice with CSF1R inhibition had similar effects to the loss of one *Csf1r* allele, with reductions seen in both SV2A and Bassoon, but not Synaptophysin, puncta (Fig. 5, A to H). Treatment with the higher, microglia-depleting dose of PLX5622 (Fig. 2, F to I) did not induce these same reductions in cortical SV2a^{+} or Bassoon^{+} puncta number, illustrating the difference between altering microglial function with partial CSF1R inhibition via low-dose CSF1Ri (150 ppm of PLX5622) and completely eliminating the microglial compartment with more extensive CSF1R inhibition (1200 ppm of PLX5622). As with the restorative effects on behavior and microglial phenotype, CSF1Ri increased presynaptic puncta in CSF1R$^{+/-}$ mice [interaction: $F(1,16) = 3.582$ $P = 0.07$; $F(1,20) = 110.5$ $P = 0.0001$; and $F(1,20) = 24.76$ $P = 0.0001$ for Synaptophysin, SV2a, and Bassoon, respectively, significance between groups displayed on graph]. Similarly, CSF1R$^{+/-}$ mice showed robust reductions in SS Ctx PNNs, which were reversed back to WT levels by CSF1Ri in CSF1R$^{+/-}$ mice [interaction: $F(1,25)$ $P = 0.48$ and $F(1,18)$ $P = 0.0003$ for WFA and aggrecan, respectively, significance between groups displayed on graph; Fig. 5, I to L], while CSF1R$^{+/-}$ mice showed markedly increased CS-56 immunofluorescence CSPGs throughout the brain that were also normalized to WT levels with CSF1Ri [interaction: $F(1,31) = 11.17$ $P = 0.0022$ significance between groups displayed on graph; Fig. 5, M and N]. Again, we noted no changes to astrocyte density or glial fibrillary protein (GFAP) immunofluorescence throughout the groups (fig. S5, M and N).

Given the changes in synaptic densities with CSF1R manipulation, and as cerebral atrophy is a feature of ALSP, we next explored neuronal densities in CSF1R$^{+/-}$ mice. While unexplored in ALSP, CSF1R has been shown to be necessary for the differentiation of

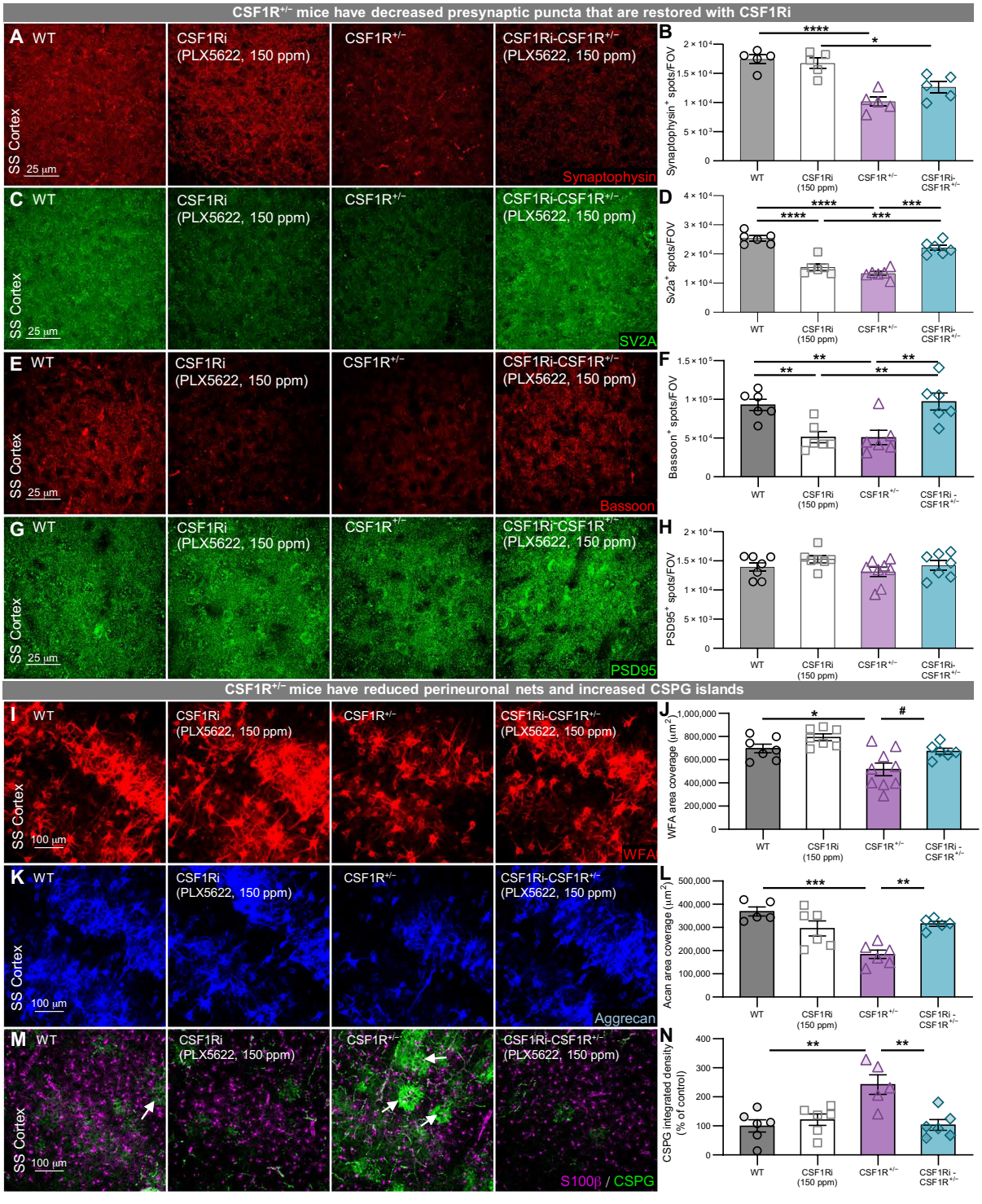

Fig. 5. Microglial dyshomeostasis results in deficits in presynaptic elements, PNN loss, and CSPG accumulation in CSF1R$^{+/-}$ SS Cortex that are restored by CSF1Ri. (**A** and **B**) Representative 63× images of SS Cortex reveal decreases in Synaptophysin puncta in CSF1R$^{+/-}$ and CSF1Ri-CSF1R$^{+/-}$ mice (**C** and **D**), decreases in SV2A in CSF1Ri and CSF1R$^{+/-}$ mice and recovery in CSF1Ri-CSF1R$^{+/-}$ mice (**E** and **F**), decreases in Bassoon in CSF1Ri and CSF1R$^{+/-}$ mice and recovery in CSF1Ri-CSF1R$^{+/-}$ mice (**G** and **H**), and no changes to PSD95 puncta. (**I**) Representative 20× images of SS Cortex from WT, CSF1Ri, CSF1R$^{+/-}$, and CSF1Ri-CSF1R$^{+/-}$ mice immunostained for WFA. (**J**) Quantification of WFA area coverage revealed a significant decrease in WFA coverage in CSF1R$^{+/-}$ SS Cortex and a trending recovery in the CSF1Ri-CSF1R$^{+/-}$ group. (**K**) Representative 20× confocal images of aggrecan immunostaining, another component ECM PNN quantification of which (**L**) revealed similar significant decreases in area coverage in the CSF1R$^{+/-}$ group and significant recovery in CSF1Ri-CSF1R$^{+/-}$ group. (**M**) Immunofluorescence of CSPG in the SS Cortex and quantification by integrated density (**N**) revealed accumulation of CSPG deposits in CSF1R$^{+/-}$ groups that was restored upon CSF1Ri. Statistical analysis used a two-way ANOVA with Sidak multiple comparisons correction. Significance is indicated as *$P < 0.05$; **$P < 0.01$; ***$P < 0.001$; ****$P < 0.0001$; #$0.05 < P < 0.1$.

Cux1$^+$ and Ctip2$^+$ neurons as CSF1R-null humans (*24*), mice (*23*), and zebrafish (*24*) displayed reductions in these neuronal subtypes. Analysis of neuronal subtype numbers (via NeuN$^+$, Cux1$^+$, and Ctip2$^+$ neurons) revealed no changes between groups (fig. S5, A to F), suggesting that neuronal loss is not present in 8-month-old CSF1R$^{+/-}$ mice. Investigation of white matter via immunolabeling for oligodendrocytes, oligodendrocyte precursor cells, and MBP revealed no changes in cell number or integrated signal density between groups (fig. S5, G to L).

CSF1Ri restores microglial homeostasis and ECM structures in pathological CSF1R$^{+/-}$ mice

To address whether CSF1Ri treatment could reverse pathology induced by *Csf1r* haploinsufficiency in more advanced stages of disease, we treated WT and CSF1R$^{+/-}$ mice with the modulatory low dose of CSF1Ri for 2 months starting at 14 months (Fig. 6A). As before, CSF1R$^{+/-}$ mice displayed cognitive impairments as assessed by NOR and NPR tasks (Fig. 6, B and C). Here, however, CSF1Ri-CSF1R$^{+/-}$ mice did not display improvements in performance [interaction: $F(1,35) = 0.7696$ $P = 0.38$ and $F(1,35) = 2.934$ $P = 0.09$ for NOR and NPR, respectively, significance between groups displayed on graph; Fig. 6, B and C] in contrast to the 8-month-old cohort wherein CSF1Ri treatment improved NOR performance in CSF1R$^{+/-}$ mice (Fig. 3C). Analysis of the brain microglial population in this more advanced cohort of mice revealed that, unlike at 8 months, 16-month-old CSF1R$^{+/-}$ mice did not display an increase in cortical microglial density compared to WT mice [interaction: $F(1,20) = 0.5908$ $P = 0.45$ significance between groups displayed on graph; Fig. 6, D and E]; however, marked microgliosis was now evident in the cc and was normalized with CSF1Ri treatment [interaction: $F(1,19) = 24.48$ $P = 0.0001$ significance between groups displayed on graph; Fig. 6, H and I]. P2RY12 expression remained diminished in CSF1R$^{+/-}$ microglia at 16 months but was again normalized with CSF1Ri [interaction: $F(1,22) = 38.74$ $P = 0.0001$ significance between groups displayed on graph; Fig. 6, F and G].

White matter impairments and loss in the cc are an established feature of disease in patients with ALSP (*2*, *3*, *7*) and CSF1R$^{+/-}$ mice (*12*, *51*). Therefore, we immunostained for MBP in the brains of these more advanced CSF1R$^{+/-}$ mice and observed similar decreases in MBP signal in both the cc and SS Ctx (Fig. 6, J and K). Statistical analyses revealed an interaction between treatment and genotype, suggesting an impact on white matter damage [interaction: $F(1,19) = 3.807$ $P = 0.06$ and $F(1,34) = 7.455$ $P = 0.01$ for cc and SS Ctx, respectively, significance between groups displayed on graph; Fig. 6, J and K]. Given the increasing relevance of neurofilament light chain (Nf-L) as a biomarker for axonal injury, we immunostained for Nf-L and noted a marked increase in the intensity of Nf-L in CSF1R$^{+/-}$ mice, which was reduced by ~30% in CSF1Ri-CSF1R$^{+/-}$ mice [interaction: $F(1,31) = 3.274$ $P = 0.08$ significance between groups displayed on graph; Fig. 6, L and M]. Sixteen-month-old CSF1R$^{+/-}$ mice displayed enduring PNN loss that was partially restored with CSF1Ri as assessed by WFA and aggrecan immunolabeling (Fig. 6, N and O). Reduced PNNs were also evident in CSF1Ri-treated WT mice at 16 months despite no such changes following CSF1Ri at 8 months of age [interaction: $F(1,18) = 15.53$ $P = 0.001$ and $F(1,19) = 26.88$ $P = 0.0001$ for WFA and aggrecan, respectively, significance between groups displayed on graph; Fig. 6, N and O]. These data suggest that, while sustained early intervention with CSF1Ri may be more efficient in preventing the overt CNS damage seen here, treatment during pathological phases still induces beneficial effects to CNS health.

Partial disruption of CSF1R signaling induces dysregulation of microglial transcripts and downstream changes in neuronal gene expression

To elucidate the mechanisms by which CSF1R signaling could both perturb and rescue cortical-dependent cognition, we performed RNA sequencing (RNA-seq) on microdissected cortices from WT, CSF1Ri, CSF1R$^{+/-}$, and CSF1Ri-CSF1R$^{+/-}$ mice. Fragments per kilobase of transcript per million mapped reads for each gene, as well as false discovery rate values for the relevant comparisons, can be explored at http://rnaseq.mind.uci.edu/green/csf1r_hets/. To explore the relationships of gene expression changes in a network, we used weighted gene coexpression network analysis (WGCNA) and identified 16 independent modules. The correlation of each module to either genotype (Fig. 7D) or CSF1Ri (Fig. 7F) highlighted several modules of interest—in particular, the brown module was highly correlated to genotype (i.e., CSF1R$^{+/-}$ mice), the darkgrey module was highly correlated to CSF1Ri, and the midnightblue module was correlated to both (correlation scores of >0.5). Eigengenes were calculated and plotted for each group for each of the three highlighted modules, alongside a heatmap of all of the genes in the module (Fig. 7, D, F, and H), and gene ontology analyses (Fig. 7, E, G, and I). The CSF1R$^{+/-}$-associated brown module was enriched for neuronally expressed genes, associated with axonogenesis, neuronal morphologies, and development, while the midnightblue module (associated with CSF1Ri-treated CSF1R$^{+/-}$ mice) is strongly enriched for genes associated with translation but not associated with any particular cell type. The CSF1Ri treatment–associated darkgrey module is enriched in microglial-expressed and immune-related genes as expected (Fig. 7, F and G), and hub genes include homeostatic microglial genes such as *C1qa*, *C1qb*, *Cd53*, *Ctss*, *Gpr34*, *P2ry12*, *Tmem119*, and *Siglech* (Fig. 7J). Normalizing these myeloid-expressed genes to microglial densities reveals a clear down-regulation of microglial transcripts in CSF1R$^{+/-}$ mice (Fig. 7, K to M), consistent with a loss of homeostasis (established homeostatic genes bolded; Fig. 7M), as well as a group of genes that are up-regulated with CSF1Ri (Fig. 7L).

We next compared differentially expressed genes (DEGs) between WT and CSF1Ri mice and WT and CSF1R$^{+/-}$ mice. Notably, 34% (412 genes) of DEGs were common between the two comparisons, with CSF1R$^{+/-}$ mice having 705 unique DEGs and CSF1Ri only 65 (Fig. 7N), suggesting similar transcriptional effects between genetic *Csf1r* haploinsufficiency and low-grade pharmacological inhibition of CSF1R. Consistent with the darkgrey module from the WGCNA analyses, down-regulated DEGs in WT versus CSF1Ri (Fig. 7O) or CSF1R$^{+/-}$ mice versus CSF1Ri-CSF1R$^{+/-}$ mice (Fig. 7Q) represented myeloid-expressed genes, as expected given the loss of ~20% of microglia with CSF1Ri. However, few myeloid-expressed DEGs were found in comparing WT to CSF1R$^{+/-}$ mice despite CSF1R$^{+/-}$ mice exhibiting ~25% higher microglial densities throughout the brain. In addition to an overall reduction in myeloid-expressed genes, these data also suggest a lack of transcripts canonically expressed by reactive or activated microglia (i.e., *Cst7*, *Clec7*, *Tnf*, *Ldl*, and *Ifitm3*), further emphasizing that disease microglia do not undergo stereotypical classical activation. Intriguingly, given the microglial expression of CSF1R, these down-regulated DEGs were far fewer in number than up-regulated DEGs either with CSF1Ri or in CSF1R$^{+/-}$ mice, as shown in volcano plots (Fig. 7, O and P). Top DEGs were similar for both comparisons and included the circadian rhythm–associated gene *NOCT*, as well as *LAMP1*, *FAM43b*, *Prr18*, and *Wrnip1*. Gene ontology analyses of DEGs between WT and CSF1R$^{+/-}$ mice highlighted

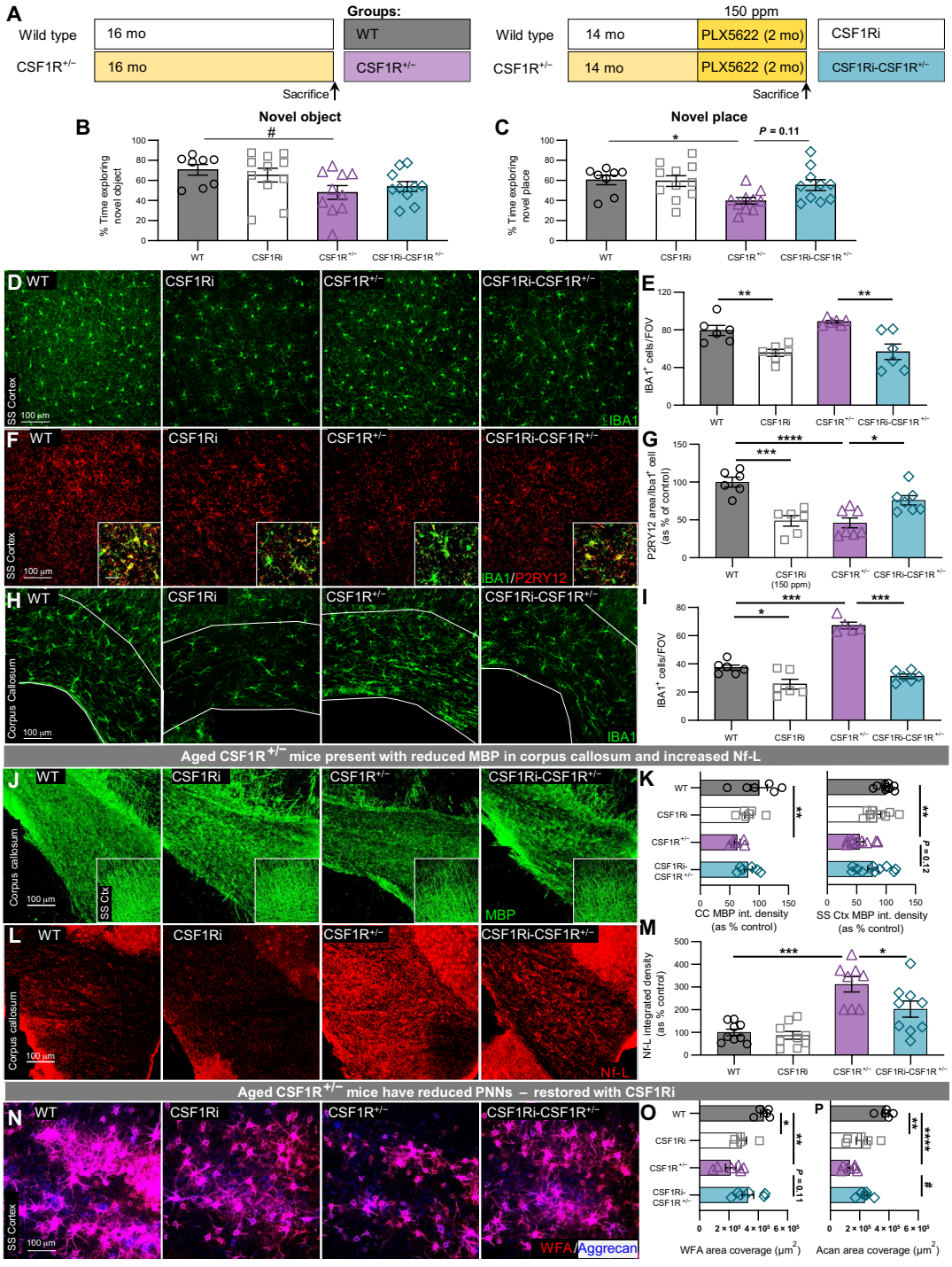

Fig. 6. Advanced-stage CSF1R$^{+/-}$ displays losses in homeostatic P2RY12 expression, MBP, and ECM immunostaining. (**A**) Experimental paradigm: WT and CSF1R$^{+/-}$ mice were treated with 150 ppm of PLX5622 for 2 months beginning at 14 months. Mice were sacrificed at 16 months ($n = 9$ to 10 per group). (**B**) CSF1R$^{+/-}$ mice trended toward exploring the novel object with less time compared to WT mice. (**C**) CSF1R$^{+/-}$ mice spent significantly less time exploring an object moved to a novel place compared to WT mice. (**D** and **E**) Representative 20× images of the SS Cortex show no differences in number of Iba1^{+} cells between aged WT and CSF1R$^{+/-}$ mice. CSF1Ri reduced Iba1^{+} cells. (**F** and **G**) Representative 20× image of the SS Cortex reveals a marked decrease in microglial P2RY12 immunopositivity in CSF1Ri and CSF1R$^{+/-}$ mice. CSF1Ri of CSF1R$^{+/-}$ mice revealed a trending increased expression in P2RY12 expression. (**H** and **I**) Representative 20× images of the cc reveal marked microgliosis in CSF1R$^{+/-}$ mice that is corrected with CSF1Ri treatment. (**J** and **K**) Representative 20× images of the cc and SS Cortex (insets) reveal marked decrease in MBP immunostaining in CSF1R$^{+/-}$ mice. (**L** and **M**) Representative 20× images of the cc reveal increased immunostaining of Nf-L in CSF1R$^{+/-}$ mice and resolution in CSF1R-CSF1R$^{+/-}$ mice. (**N** to **P**) Representative 20× images of WFA and aggrecan immunostaining reveal marked decrease in staining for both in CSF1Ri and CSF1R$^{+/-}$ mice. CSF1Ri-CSF1R$^{+/-}$ mice had trending increases for both. Statistical analysis used a two-way ANOVA with Sidak multiple comparisons correction. Significance: *$P < 0.05$; **$P < 0.01$; ***$P < 0.001$; ****$P < 0.0001$; #$0.05 < P < 0.1$.

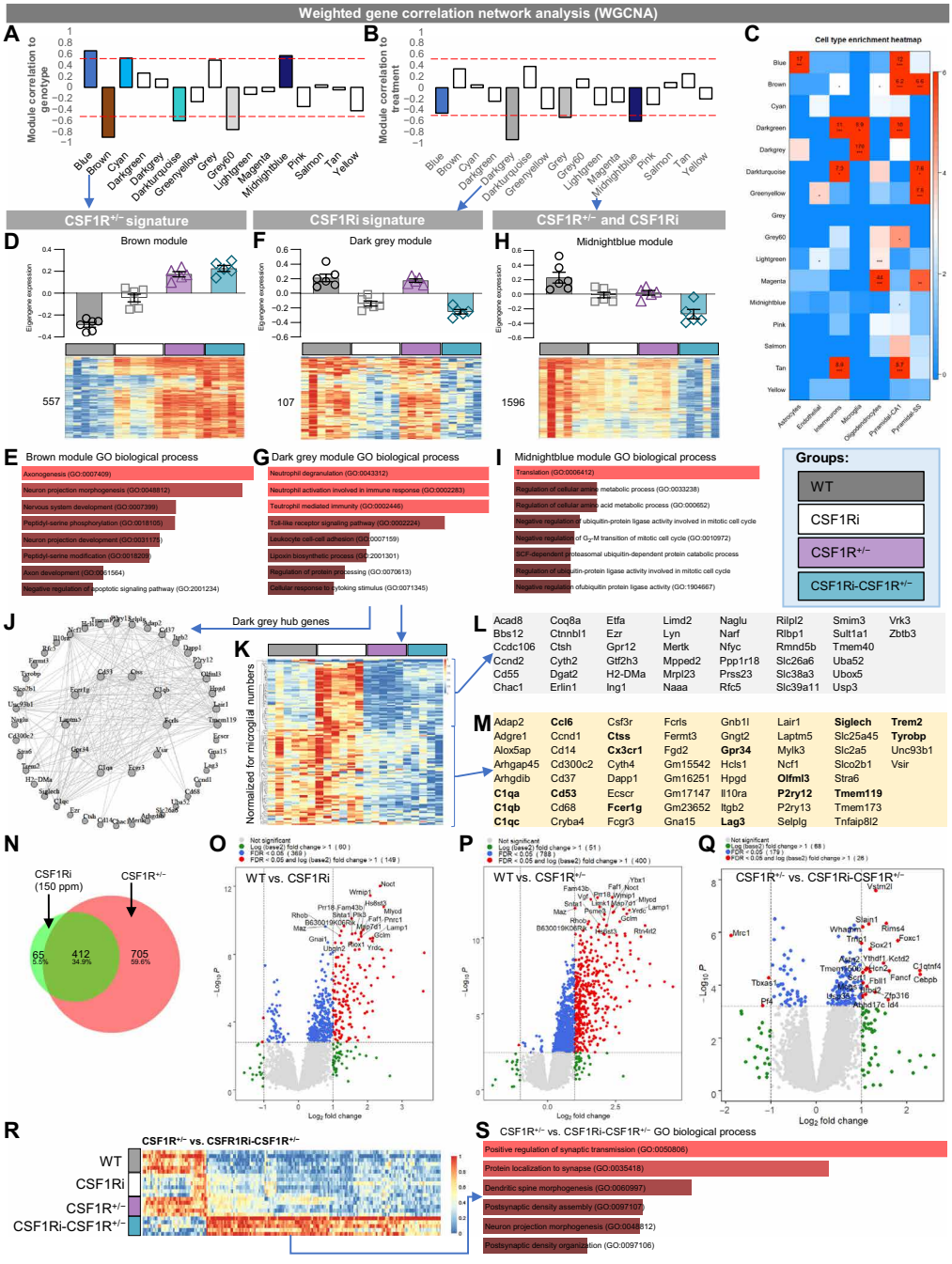

Fig. 7. CSF1R signaling disruptions induce loss of microglial homeostasis but primarily affect neuronal gene expression. (**A**) Correlation of coexpression modules to genotype (*z* score cutoff, ±0.5). (**B**) Correlation of modules to treatment (*z* score cutoff, ±0.5). (**C**) Cell type enrichment heatmap of coexpression modules. Values provided indicate the number of genes within network associated with that specific cell type. ***6+ genes; **3+ genes. (**D** and **E**) CSF1R$^{+/-}$ signature: Module eigengene trajectory and heatmap of gene expression value (D) and gene ontology (GO) term enrichment for brown module (E). (**F** and **G**) CSF1Ri signature: Module eigengene trajectory and heatmap of gene expression value (F) and GO term enrichment for the darkgrey module (G). (**H** and **I**) CSF1Ri and CSF1R$^{+/-}$ signature: Module eigengene trajectory and heatmap of gene expression value (H), as well as GO term enrichment for midnightblue module (I). Curated GO grids ranked on the basis of pathway *P* value where cutoff was 0.05. Colors are associated with an adjusted *P* value cutoff of 0.1 wherein pathways with lighter color have lower adjusted *P* value. (**J**) Interaction plot showing hub genes from the darkgrey module shows distinct CSF1Ri signature. (**K**) Heatmap of genes in the darkgrey module normalized to average microglial numbers found within a group. (**L**) List of up-regulated genes in CSF1Ri-CSF1R$^{+/-}$ compared to CSF1R$^{+/-}$ mice. (**M**) List of down-regulated genes between WT and CSF1R$^{+/-}$ mice normalized for number of microglia. (**N**) Venn diagram displaying the number of DEGs generated in transcriptional comparisons between CSF1Ri mice and CSF1R$^{+/-}$ mice in comparison with WT mice. (**O** to **Q**) Volcano plots displaying fold change of genes ($\log_2$ scale) and *P* values ($-\log_{10}$ scale) between WT and CSF1Ri mice (O), WT and CSF1R$^{+/-}$ mice (P), and CSF1R$^{+/-}$ and CSF1Ri-CSF1R$^{+/-}$ (Q). (**R**) Heatmap of DEGs between CSF1R$^{+/-}$ and CSF1Ri-CSF1R$^{+/-}$ mice. (**S**) Top biological GO term enrichment for up-regulated genes from heatmap (R). FDR, false discovery rate.

axonogenesis (fig. S6B) and similarities to gene changes in spinal cord injury and HD (fig. S6C), both of which have been shown to involve profound ECM remodeling, resembling what we see in the context of *Csf1r* haploinsufficiency (*20*, *59*, *60*). Furthermore, all up-regulated DEGs induced by either CSF1Ri in WT mice or comparing WT to CSF1R$^{+/-}$ mice appear to be neuronally expressed. These data suggest that, despite CSF1R being restricted to microglia in the adult brain, altered CSF1R signaling in microglia induces robust gene expression changes in neurons.

To understand how CSF1Ri of CSF1R$^{+/-}$ mice could rescue disease-related impairments in synaptic integrity, ECM remodeling, and cognition, we performed more comprehensive analyses of DEGs between CSF1R$^{+/-}$ and CSF1Ri-treated CSF1R$^{+/-}$ mice (Fig. 7, Q and R). The most significantly down-regulated gene was *MRC1*, a myeloid-expressed gene associated with phagocytosis (*61*). Conversely, most DEGs are up-regulated in CSF1Ri-treated CSF1R$^{+/-}$ mice, as depicted in Fig. 7R. Gene ontology analyses of these DEGs highlight their roles in synaptic function and morphology (Fig. 7R), confirming changes to synapses that could account for the changes in synaptic landscape that we have observed here. Collectively, from these analyses, we conclude that there is a loss of microglial homeostatic signature in CSF1R$^{+/-}$ mice, rather than a reactive or activated signature.

DISCUSSION

Accumulating evidence indicates that microglia are critically involved in neurodegenerative disease progression. However, it remains unclear whether these cells play a causative role in driving disease pathology and neurodegeneration, a reactive role by responding harmfully to existing pathology, or both. CNS disorders that present genetic etiologies linked to microglia-specific genes provide unique opportunities to investigate and answer these questions (e.g., how microglia drive brain disease). While these disorders have been reported, the cellular mechanisms by which these underlying genetic disturbances lead to overt CNS pathology remain largely unknown. In this study, we conditionally induced microglial *Csf1r* haploinsufficiency in adult mice to explore the role of partially disrupted CSF1R signaling on microglial homeostasis and CNS function. In addition, we used a constitutive mouse model of *Csf1r* haploinsufficiency and explored the consequences of low-grade modulatory and high-grade microglia-depleting doses of the pharmacological CSF1R inhibitor PLX5622. It is important to stress that CSF1R inhibition is highly dynamic—sustained, potent inhibition can eliminate the entire microglial compartment for the duration of treatment, while low-grade inhibition modulates microglial activity/function in a dose-dependent manner, with less extensive depletion of the microglial population (*62*). For this reason, and because sustained loss of the adult microglial pool is not clinically viable in the long term, a modulatory dose of PLX5622 for low-grade CSF1R inhibition was used to assess how pharmacologically impairing CSF1R signaling in healthy adult mice (or further inhibiting this pathway in *Csf1r* haploinsufficient mice) influences CNS homeostasis in the presence of microglia.

To establish whether postdevelopmental *Csf1r* haploinsufficiency in microglia was sufficient to induce pathology, we used a tamoxifen-inducible Cre recombinase system in which one floxed copy of the *Csf1r* allele was conditionally excised in adult CX3CR1^{+} microglia (iCSF1R$^{+/-}$ mice). As human patients with ALSP are *Csf1r* haploinsufficient from birth, we validated our findings in an additional constitutive CSF1R$^{+/-}$ model. We noted a loss of microglial P2RY12 expression following iCSF1R$^{+/-}$ tamoxifen recombination and in CSF1R$^{+/-}$ mice, conventionally reflective of a loss of microglial homeostasis in disease (*30*–*32*) and similar to the down-regulation of P2RY12 expression in human patients with ALSP harboring *Csf1r* mutations (*34*). Accordingly, our RNA-seq data revealed a general down-regulation of canonical microglial gene expression, consistent with a departure from homeostasis. We were also unable to detect an enrichment of inflammatory gene transcripts associated with microglial activation (e.g., *Cst7*, *Axl*, or *Ldl*, as seen in damage-associated microglia) (*30*). The phenotypes of CSF1R$^{+/-}$ microglia that we describe here resemble those that we recently reported in a mouse model of HD (*20*), as supported by gene ontology analysis of WT versus CSF1R$^{+/-}$ gene enrichment (fig. S6C). These results suggest that phenotypic states of microglia independent from traditional paradigms of immune activation may also contribute negatively to disease outcome. It should be noted that CSF1Ri did not rescue deficits in NPR tasks (Fig. 3D). NPR memory has been critically linked to hippocampal activity (*64*), as opposed to the cortical dependence of tasks like NOR (*65*, *66*). These results informed our decision to specifically focus on cortical regions for subsequent analyses. However, future studies should explore the divergent effects of CSF1Ri on myeloid populations among various regions of the CNS, especially with regard to their effects on CNS health.

Further, our data emphasize the concept of the tetrapartite synapse as a particularly disease-relevant neurological unit, in which synaptic structure and function are regulated by four key elements: pre- and postsynaptic compartments, glial cells, and the ECM. With regard to this, we observed a consistent down-regulation or elimination of presynaptic markers (Sv2a, Bassoon, and Synaptophysin) in iCSF1R$^{+/-}$ (Fig. 1) and CSF1R$^{+/-}$ mice (Fig. 5), while postsynaptic proteins (PSD95) appeared to be spared. This is consistent with microglial trogocytosis of synaptic elements (e.g., partial engulfment by microglia of target substrate rather than complete phagocytosis), whereby microglia sculpt presynaptic elements to refine neural circuits while sparing postsynaptic components (*19*). In terms of the ECM, we observed deficits in PNNs, specialized lattice-like structures composed of CSPGs that provide structural and biochemical stability to proximal synapses (*67*). Genetic or enzymatic modifications to PNN composition induce changes in synapse number (*68*, *69*), transmission (*70*), and receptor makeup (*71*), and hence, these structures play a critical role in regulating synaptic connectivity and plasticity (*41*, *42*). Furthermore, PNNs augment neuronal excitability/firing (*72*) and protect neurons against neurotoxins (*73*). We recently reported microglia-facilitated loss of PNNs as a general feature of neurodegeneration in HD (*20*) and AD (*44*). Here, we highlighted a loss of microglial homeostasis following induction of *Csf1r* haploinsufficiency, whether genetic (iCSF1R$^{+/-}$ or CSF1R$^{+/-}$) or pharmacological, that was concomitant with reductions in presynaptic puncta and disruptions to ECM structures, strongly supporting a microglial origin for these deficits.

In support of this microglial basis of pathology, we found that elimination of the microglial compartment (with sustained high-dose CSF1R inhibition) prevented both loss of presynaptic surrogates and PNNs and disease-related CSPG deposition in CSF1R$^{+/-}$ mice. Crucially, these results suggest that specific targeting of microglia can prevent *Csf1r* haploinsufficiency–associated CNS damage and demonstrate how altered microglial phenotypes can exert profound effects on neuronal function. A caveat of our experiments is that we focused

our analyses on microglial populations in the CNS. As mentioned previously, macrophages that also express *Csf1r*, such as PVMs, could theoretically play a role in inducing pathology given their involvement in the maintenance of steady-state tissue (*67*) and should be explored in future studies. That being said, we believe that microglia are the most likely culprits for the pathology observed here. Our findings also demonstrate that CSF1R signaling deficiency, either via genetic haploinsufficiency or CSF1Ri, leads to microglial dyshomeostasis, further suggesting that CSF1R is a critical regulator of homeostatic function in microglia. We observed overlapping phenotypes induced by CSF1Ri in WT mice and genetic haploinsufficiency in CSF1R$^{+/-}$ mice, e.g., down-regulation of P2RY12 expression in microglia, and loss of presynaptic puncta. RNA-seq analyses also showed ~34% overlap in DEGs between CSF1Ri and *Csf1r* haploinsufficiency, and notably, most of these genes were of neuronal origin. In older WT animals, CSF1Ri treatment led to PNN loss that was not present in younger mice, perhaps suggesting an increased vulnerability to disruptions in CSF1R signaling with age. These data emphasize how changes in microglial phenotype can modulate neuronal gene expression, function, and structure and link genetic and pharmacological impairments in CSF1R signaling to specific changes in microglial homeostasis, synaptic integrity, and ECM organization.

In this study, we also reported paradoxical observations whereby inhibiting CSF1R signaling in a system already deficient in *Csf1r* leads to recovery, rather than exacerbation, of multiple facets of CNS homeostasis. This included improved cognitive performance and normalization of microglial phenotypes (densities, morphologies, and P2RY12 expression), PNNs, CSPGs, and presynaptic puncta. Furthermore, RNA-seq data highlighted marked increases in neuronal- and synaptic-associated genes with CSF1Ri in CSF1R$^{+/-}$ cortices, such as *Syn2*, *Begain*, and *Rims3*. Prior studies using CSF1R inhibitors in mouse models of AD and MS (Multiple Sclerosis) have also shown modulatory effects on neurodegenerative pathologies (*55*, *74*, *75*). In parallel with our findings, restoration of microglial homeostasis by genetic knockout of a single *Csf2* allele in CSF1R$^{+/-}$ mice, which exhibit increased *Csf2* mRNA expression, prevented loss of myelin and reversed CSF1R$^{+/-}$ behavioral deficits in CSF1R$^{+/-}$ mice by reinstating balanced CSF1R/CSF2 signaling (*51*). While a genetic approach to normalizing microglial homeostasis is attractive in its specificity, the pharmacological approach of CSF1Ri presents an alternative to targeting this pathway with its own unique advantages (e.g., CSF1R inhibitors can be used at virtually any time and for any duration, can be titrated as desired, and readily cross the blood-brain barrier). It is important to note that while haploinsufficiency is considered by some to be a valid model of ALSP, given the emergence of human patients with ALSP with *Csf1r* haploinsufficiency (*2*, *11*), there is still debate on how haploinsufficiency may account for all cases of ALSP (*76*–*78*). A vast number of ALSP mutations result in kinase dead receptors leading to a dominant-negative phenotype (*8*, *77*, *79*). While in our study, treatment of *Csf1r* haploinsufficient mice managed to reverse pathology, further studies are necessary to explore how CSF1Ri would affect kinase dead mutations.

Constitutive CSF1R haploinsufficiency resulted in elevated microglial densities in adult mice, in line with prior reports (*12*, *51*), including in microglia-specific CSF1R haploinsufficient mice (*58*). In line with an impaired developmental establishment of the microglial population, we find that microglial densities were not increased in adult iCSF1R$^{+/-}$ mice; despite this, induction of microglial-specific CSF1R haploinsufficiency in the adult was sufficient to cause loss of microglial homeostasis and associated loss of presynaptic puncta and remodeling of the ECM, indicating that increased microglial number does not contribute to the pathology observed here. Accordingly, discrepancies exist between microglial densities reported in constitutive CSF1R haploinsufficient mice and CSF1R haploinsufficient rats (*76*) and zebrafish (*26*), which do not show these increases, while studies in postmortem human ALSP brains suggest an initial increase in microglial densities followed by later reductions (*3*). Similarly, we find that older Csf1r$^{+/-}$ mice no longer have increased cortical microglial densities, suggesting similar age-related reductions in microglia number in these mice. These data further suggest that changes in microglial densities, at least in mice, are not key drivers of pathology but that it is altered microglial phenotypes induced by a loss of a *Csf1r* allele that are important.

It should be highlighted that there is a marked difference in the effects of CSF1Ri that modulate microglial phenotypes versus microglia-depleting doses—none of the neuronal gene changes seen in the context of genetic or pharmacological *Csf1r* haploinsufficiency are observed in MD-WT mice [http://rnaseq.mind.uci.edu/green/ad_plx/; (*20*, *27*)] nor are reductions in synaptic puncta seen (Fig. 2, D to G). Similarly, elimination of microglia from healthy adult mice in a prior study does not confer ALSP pathology (i.e., cognitive deficits, PNN degradation, and synaptic loss), despite 6 months of microglial depletion (*27*). Microglial depletion is generally associated with improved performance in memory and cognitive tasks (*25*, *27*, *80*). Moreover, our data, with respect to MD-CSF1R$^{+/-}$ pathology recovery, provide further evidence of these cells being viable targets for therapeutic intervention especially at early stages of disease onset. The recent development of the *Csf1r*$^{\Delta FIRE/\Delta FIRE}$ mouse line (*81*) and *Csf1r* $^{-/-}$ rats (*82*), which do not develop microglia in the brain but are otherwise healthy, further suggests at least partial functional redundancy in the maintenance of adult CNS homeostasis by microglia. Collectively, our results indicate that improperly functioning or "dyshomeostatic" microglia are worse for the adult brain under baseline conditions than the lack of microglia altogether (*31*, *63*).

MATERIALS AND METHODS

Compounds

PLX5622 was provided by Plexxikon Inc. and formulated in AIN-76A standard chow at a dose of 150 or 1200 ppm by Research Diets Inc.

Mice

All mice were obtained from the Jackson laboratory. Mice were mixed-sex C57BL/6 (000664) mice. Animals were housed with open access to food and water under 12-hour/12-hour light-dark cycles. All mice were aged to 8 months unless otherwise indicated. *Csf1r*$^{+/-}$ mice were provided by K. Cramer (University of California, Irvine; Department of Neurobiology and Behavior) and were maintained and genotyped as described previously (*77*). For genotyping *Csf1r*$^{+/-}$ mice, the following primers were used: forward, 5′ ATCCAGCATTAGGCAGCCT; reverse, 5′ GCCACCATGTGTCCGTGCTT. For inducible CSF1R haploinsufficiency experiments, the following mice were obtained from the Jackson laboratory: CSF1R$^{fl/fl}$ (B6.Cg-*Csf1r*$^{tm1.2Jwp}$/J; stock no. 021212) and Cx3Cr1$^{cre\text{-}ert2/cre\text{-}ert2}$ [B6.129P2(C)-Cx3cr1$^{tm2.1(cre/ERT2)Jung}$; stock no. 020940]. Progeny

from these mice were bred to produce groups of interest. For genotyping *Csf1r*$^{+}$/*Csf1r*^{fl} mice, the following primers were used: forward, 5′ CTGGACTCATCCACCACCTT; reverse, 5′ CGTTGGCTACCCGTGATATT. For genotyping *Cx3cr1*$^{cre\text{-}ert2}$ mice, the following primers from the Jackson laboratory were used: WT forward, 5′ AGCTCACGACTGCCTTCTTC; common, 5′ ACGCCCAGA CTAATGGTGAC; mutant forward, 5′ GTTAATGACCTGCAGCCAAG.

Animal treatments

All rodent experiments were performed in accordance with animal protocols approved by the Institutional Animal Care and Use Committee at the University of California, Irvine. The CSF1R$^{+/-}$ mouse model (*12*, *51*) has been previously described in detail. For lipopolysaccharide (LPS) experiments, 9-month-old male and female WT mice were intraperitoneally injected with LPS (0.5 mg/kg), as described before (*25*), (L4130, Sigma-Aldrich) and BrdU (5-bromo-2′-deoxyuridine; 000103, Thermo Fisher Scientific) or saline and BrdU every other day for a week followed by euthanasia 24 hours after the last dose. BrdU injections were intraperitoneally administered to all mice at a dose of 1 ml/100 g of body weight (*25*) (per the manufacturer's instructions) twice daily. At the end of treatments, mice were euthanized via CO_2 inhalation and transcardially perfused with 1× phosphate-buffered saline (PBS). For all studies, brains were removed, and hemispheres separated along the midline. Brain halves were either flash-frozen for subsequent biochemical analysis or drop-fixed in 4% paraformaldehyde (PFA; Thermo Fisher Scientific, Waltham, USA) for subsequent immunohistochemical analysis. Half brains were collected into 4% PFA for 48 hours and then transferred to a 30% sucrose solution with 0.02% sodium azide for another 48 to 72 hours at 4°C. Fixed half brains were sliced at 40 μm using a Leica SM2000 R freezing microtome. The flash-frozen hemispheres were microdissected into cortical, hippocampal, and thalamic/striatal regions and then ground with a mortar and pestle to yield a fine powder. For RNA analyses, half of the powder was processed with an RNAeasy Plus Universal Mini Kit (Qiagen, Valencia, USA) according to the manufacturer's instructions.

Behavioral assays

The following behavioral paradigms were carried out in the following order (*25*). WT and CSF1R$^{+/-}$ underwent behavioral assessment 6 weeks after being placed on their respective diet beginning at 6 months.

Elevated plus maze

Mice were placed in the center of an EPM for 5 min to assess anxiety. Unless otherwise stated, ANY-Maze software was used to video-record and track animal behavior. The total number of open and closed arm entries and the time spent in each arm were determined.

Open field

In brief, mice were placed in a white box for 5 min to assess anxiety. The amount of time spent in the center versus the perimeter of the arena was obtained. Measurements on distance traveled and average speed of the mice were also observed. Notably, the same arena was used for OF, novel object, novel place, and social interaction tasks.

Novel object recognition

Mice were allowed to freely explore two identical objects (either small glass beakers or plastic building blocks; counterbalanced for treatment), and exploratory behavior was recorded for 5 min. Twenty-four hours later, one familiar object is replaced with a novel object (either beaker or block), and behavior is recorded for 3 min. The amount of time spent investigating the novel object was determined by calculating the discrimination index (time investigating novel object – time investigating old object/total time) and is presented as a percentage, where chance level of investigation for each object is 50%.

Novel place recognition

Mice were allowed to freely explore two identical objects (either small glass beakers or plastic building blocks; counterbalanced for treatment), and exploration behavior is recorded for 5 min. Twenty-four hours later, one familiar object is moved to a new location, and behavior is recorded for 3 min. The amount of time spent investigating the novel object was determined by calculating the discrimination index (time investigating novel place—time investigating old place/total time) and is presented as a percentage, where chance level of investigation for each place is 50%.

Social interaction task

Mice were allowed to freely explore the arena for 5 min. After habituation, a control mouse of the same sex was placed inside a wire containment cup that is located to the side of the arena. Subject mouse was allowed free access to the arena and control mouse for 5 min. The number of direct contacts between the subject mouse and the containment cup housing a control mouse was quantified as active contacts. Duration of active contact points was measured and determined by calculating the discrimination index (time of active contact points/total time) and is presented as a percentage.

Rotarod

The motor capabilities of the mice were tested using an accelerating rotarod (Ugo Basile). Each mouse was placed on the rotarod beam for a maximum of 5 min while it accelerated from 8 to 40 rpm. The experimenter stopped the timer when either the mouse fell off the beam or the mouse held on to the beam and its body completed two full rotations. A total of five trials were performed per mouse, each with a 15-min intertrial interval.

Oral gavage of adult mice with tamoxifen

Tamoxifen (Sigma-Aldrich, T5648) was dissolved in corn oil (Sigma-Aldrich, C8267) at a concentration of 50 mg/ml. For adult induction of CSF1R haploinsufficiency, tamoxifen (5 mg/25 g of body weight) was orally gavaged daily for 5 days. Tamoxifen administration began at 2 months, and brains were harvested at 8 months.

Histology and confocal microscopy

For immunostaining of P2RY12, aggrecan, CSPG CS-56, and Ctip2, antigen retrieval was performed by heating the sections in citrate buffer (10 mM; pH 6.0) for 30 min at 80°C followed by a 10-min cooling period and 5-min 1× PBS wash. Fluorescent immunolabeling followed using a standard indirect technique as described previously (*27*). Brain sections were stained with primary antibodies against the following: IBA1 (1:1000; 019-19741, Wako and ab5076, Abcam), WFA (1:1000; B1355, Vector), aggrecan (1:200; ab1031, Millipore), CSPG CS-56 (1:200; ab11570, Abcam), S100β (1:200; Abcam), GFAP (1:1000; Abcam), Ki67 (1:200; Cell Signaling), BrdU (1:500; Abcam), NeuN (1:1000; Millipore), MBP (1:200; Millipore), PDGFRα (1:200; Thermo Fisher Scientific), Olig2 (1:200; Abcam), Synaptophysin (1:1000; Sigma-Aldrich), PSD95 (1:500; Abcam and Cell Signaling), Bassoon (1:1000; Synaptic Systems), P2RY12 (1:200; Sigma-Aldrich), Ctip2 (1:200; Abcam), SV2A (1:200; Synaptic Systems), Nf-L (1:200; Synaptic Systems), CD206 (1:200; Thermo Fisher Scientific), CD163 (1:200; Abcam), and CUX1 (1:200; Abcam).

For TUNEL staining, the Promega Dead End TUNEL Assay Kit (catalog no. G3250) was used following the manufacturer's instructions. Briefly, samples were washed in PBS, incubated in equilibration buffer for 10 min, and covered with plastic coverslips. Slides were then immersed in incubation buffer made of equilibration buffer (180 μl), nucleotide mix (20 μl), and rTdT enzyme (4 μl) at 37°C for 1 hour not exposed to light. Slides were dipped in 2× SSC buffer for 10 min at room temperature. Deoxyribonuclease I was used to generate strand breaks in DNA to provide a positive TUNEL reaction control. Negative control sections were incubated in incubation buffer without rTdT enzyme.

For RNAscope in situ hybridization, we followed the manufacturer's instructions. Briefly, tissue sections were mounted onto slides and warmed at 60°C for 30 min. Sections were dehydrated with 50, 70, and 100% ethyl alcohol gradients for 5 min each at room temperature and followed by hydrogen peroxide (catalog no. 322335, ACDBio) at room temperature for 10 min each and then washed with deionized (DI) water. Tissue sections were placed in boiling 1× Target Retrieval reagent (catalog no. 322380, ACDBio) for 15 min then immediately transferred to DI water and washed in 100% ethyl alcohol and allowed to dry. Slides were covered in Protease III (catalog no. 322337, ACDBio) for 30 min at 40°C. Probes were then added for 2 hours at 40°C within a humidity control chamber. Signal amplification and detection reagents (catalog no. 322310, ACDBio) were applied sequentially and incubated in AMP 1, AMP 2, and AMP for 30 min each. Before adding each AMP reagent, samples were washed twice with washing buffer (catalog no. 310091, ACDBio). Respective horseradish peroxidases (HRPs) were placed on slides for 15 min at 40°C followed by 30 min of respective Opal dye (FP1487001KT, Akoya Biosciences) for 30 min at 40°C and HRP blocker for 15 min at 40°C.

High-resolution fluorescent images were obtained using a Leica TCS SPE-II confocal microscope and LAS-X software. For confocal imaging, one field of view (FOV) per brain region was captured per mouse using the Allen Brain Atlas to capture comparable brain regions. For synaptic quantifications, three FOVs per brain region were captured, and quantifications for each animal were averaged. Total cell counts and morphological analyses were obtained by imaging comparable sections of tissue from each animal at a 20× objective, at multiple z-planes, followed by automated analyses using Bitplane Imaris 7.5 spots and filaments, respectively, as described previously (*84*). Colocalization analyses were conducted using Bitplane Imaris 7.5 colocalization and surfaces modules. For hemisphere stitches, automated slide scanning was performed using a Zeiss AxioScan.Z1 equipped with a Colibri camera and Zen AxioScan 2.3 software. Cell quantities were determined using the spots module in Imaris. Integrated density measurements were determined in ImageJ (National Institutes of Health).

RNA sequencing

Whole-transcriptome RNA-seq libraries were produced from WT, CSF1Ri, CSF1R$^{+/}$, and CSF1Ri-CSF1R$^{+/-}$ mice treated from 6 to 8 months, brains that were microdissected to extract cortical tissue (n = 6 per group). Briefly, 100 to 600 ng of RNA were depleted of ribosomal RNA, fragmented, reverse-transcribed, and ligated to indexed sequencing adapters using the KAPA RNA HyperPrep Kit with RiboErase. Amplified libraries were combined into four pools of 12 libraries and sequenced on four lanes of a HiSeq 4000 producing 50–base pair single-end reads. Reads were mapped to the reference mouse genome (mm10) using the STAR (*85*) aligner and quantified with the featureCounts function of the Rsubread (*86*) package in R (*87*). After filtering out low-count genes, count distributions were scaled using the calcNormFactors function of the edgeR (*88*) package.

Weighted correlation network analysis

Network analysis was performed using the WGCNA package in R (*83*). First, biweighted mid-correlations were calculated for all gene pairs and then used to generate an eigengene network matrix, which reflects the similarity between genes according to their expression profiles. This matrix was then raised to power β (β = 20). Modules were defined using specific module cutting parameters (minimum module size, 100 genes; deepSplit, 4; and threshold of correlation, 0.2). Modules with a correlation greater than 0.8 were merged. We used the first principal component of the module, called signed bicor network, to correlate brain region, irradiation, and treatment. Hub genes were defined using the intramodular connectivity (kME) parameter of the WGCNA package.

Gene enrichment analysis

Gene set enrichment analysis was done using enrichR (*90*).

Quantitative PCR

Complementary DNA (cDNA) was prepared using an iScript cDNA synthesis kit following the manufacturer's instructions (Bio-Rad, 1708890). Quantitative real-time PCR was performed to determine the relative expression of *Csf1r* and *Gapdh* as a control. The primer pairs for each were obtained as part of the PrimePCR-PreAMP SYBR Green Assay (Bio-Rad; unique assay IDs: qMmuCID0016567 and qMmuCED0027497). Real-time PCRs were performed in 20-μl volume reactions using the SsoAdvanced Universal Supermix SYBR Green system (Bio-Rad). Real-time PCR conditions were 95°C for 2 min for 1 cycle followed by 95°C for 10 s and 60°C for 30 s for 40 cycles on a Bio-Rad CFX96 Touch thermocycler.

Data analysis and statistics

Statistical analysis was performed with Prism GraphPad (v.8.0.1; La Jolla, USA). To compare two groups, the unpaired or paired Student's t test was used. Behavioral, biochemical, and immunohistological data were analyzed using two-way analysis of variance (ANOVA) (diet: control versus PLX5622 and genotype: WT versus CSF1R$^{+/-}$) using GraphPad Prism version 8. Tukey's post hoc tests were used to examine biologically relevant interactions from the two-way ANOVA regardless of statistical significance of the interaction. For all analyses, statistical significance was accepted at $P < 0.05$, and significance is expressed as follows: $^{*}P < 0.05$, $^{**}P < 0.01$, and $^{***}P < 0.001$. n is given as the number of mice within each group. Statistical trends are accepted at $P < 0.10$ ($^{\#}$). Data are presented as raw means and SEM.

SUPPLEMENTARY MATERIALS

Supplementary material for this article is available at http://advances.sciencemag.org/cgi/content/full/7/35/eabg1601/DC1

View/request a protocol for this paper from *Bio-protocol*.

REFERENCES AND NOTES

1. Y. Kondo, A. Matsushima, S. Nagasaki, K. Nakamura, Y. Sekijima, K. Yoshida, Factors predictive of the presence of a *CSF1R* mutation in patients with leukoencephalopathy. *Eur. J. Neurol.* **27**, 369–375 (2020).
2. T. Konno, T. Miura, A. M. Harriott, N. Mezaki, E. S. Edwards, R. Rademakers, O. A. Ross, J. F. Meschia, T. Ikeuchi, Z. K. Wszolek, Partial loss of function of colony-stimulating factor 1 receptor in a patient with white matter abnormalities. *Eur. J. Neurol.* **25**, 875–881 (2018).

3. K. Oyanagi, M. Kinoshita, E. Suzuki-Kouyama, T. Inoue, A. Nakahara, M. Tokiwai, N. Arai, J. I. Satoh, N. Aoki, K. Jinnai, I. Yazawa, K. Arai, K. Ishihara, M. Kawamura, K. Ishizawa, K. Hasegawa, S. Yagisita, N. Amano, K. Yoshida, S. Terada, M. Yoshida, H. Akiyama, Y. Mitsuyama, S. I. Ikeda, Adult onset leukoencephalopathy with axonal spheroids and pigmented glia (ALSP) and Nasu-Hakola disease: Lesion staging and dynamic changes of axons and microglial subsets. *Brain Pathol.* **27**, 748–769 (2017).
4. C. Sundal, Z. K. Wszolek, *CSF1R*-related adult-onset leukoencephalopathy with axonal spheroids and pigmented glia, in *GeneReviews®*, M. P. Adam, H. H. Ardinger, R. A. Pagon, S. E. Wallace, L. J. H. Bean, G. Mirzaa, A. Amemiya, Eds. (University of Washington, 1993).
5. M. Hiyoshi, M. Hashimoto, M. Yukihara, F. Bhuyan, S. Suzu, M-CSF receptor mutations in hereditary diffuse leukoencephalopathy with spheroids impair not only kinase activity but also surface expression. *Biochem. Biophys. Res. Commun.* **440**, 589–593 (2013).
6. A. M. Nicholson, M. C. Baker, N. A. Finch, N. J. Rutherford, C. Wider, N. R. Graff-Radford, P. T. Nelson, H. B. Clark, Z. K. Wszolek, D. W. Dickson, D. S. Knopman, R. Rademakers, CSF1R mutations link POLD and HDLS as a single disease entity. *Neurology* **80**, 1033–1040 (2013).
7. R. Rademakers, M. Baker, A. M. Nicholson, N. J. Rutherford, N. Finch, A. Soto-Ortolaza, J. Lash, C. Wider, A. Wojtas, M. DeJesus-Hernandez, J. Adamson, N. Kouri, C. Sundal, E. A. Shuster, J. Aasly, J. MacKenzie, S. Roeber, H. A. Kretzschmar, B. F. Boeve, D. S. Knopman, R. C. Petersen, N. J. Cairns, B. Ghetti, S. Spina, J. Garbern, A. C. Tselis, R. Uitti, P. Das, J. A. Van Gerpen, J. F. Meschia, S. Levy, D. F. Broderick, N. Graff-Radford, O. A. Ross, B. B. Miller, R. H. Swerdlow, D. W. Dickson, Z. K. Wszolek, Mutations in the colony stimulating factor 1 receptor (*CSF1R*) gene cause hereditary diffuse leukoencephalopathy with spheroids. *Nat. Genet.* **44**, 200–205 (2011).
8. C. Leng, L. Lu, G. Wang, Y. Zhang, Y. Xu, X. Lin, N. Shen, X. Xu, S. Qun, M. Sun, W. Ge, A novel dominant-negative mutation of the CSF1R gene causes adult-onset leukoencephalopathy with axonal spheroids and pigmented glia. *Am. J. Transl. Res.* **11**, 6093–6101 (2019).
9. S. J. Adams, A. Kirk, R. N. Auer, Adult-onset leukoencephalopathy with axonal spheroids and pigmented glia (ALSP): Integrating the literature on hereditary diffuse leukoencephalopathy with spheroids (HDLS) and pigmentary orthochromatic leukodystrophy (POLD). *J. Clin. Neurosci.* **48**, 42–49 (2018).
10. S. Hoffmann, J. Murrell, L. Harms, K. Miller, A. Meisel, T. Brosch, M. Scheel, B. Ghetti, H. H. Goebel, W. Stenzel, Enlarging the nosological spectrum of hereditary diffuse leukoencephalopathy with axonal spheroids (HDLS). *Brain Pathol.* **24**, 452–458 (2014).
11. T. Konno, M. Tada, M. Tada, A. Koyama, H. Nozaki, Y. Harigaya, J. Nishimiya, A. Matsunaga, N. Yoshikura, K. Ishihara, M. Arakawa, A. Isami, K. Okazaki, H. Yokoo, K. Itoh, M. Yoneda, M. Kawamura, T. Inuzuka, H. Takahashi, M. Nishizawa, O. Onodera, A. Kakita, T. Ikeuchi, Haploinsufficiency of *CSF-1R* and clinicopathologic characterization in patients with HDLS. *Neurology* **82**, 139–148 (2014).
12. V. Chitu, S. Gokhan, M. Gulinello, C. A. Branch, M. Patil, R. Basu, C. Stoddart, M. F. Mehler, E. R. Stanley, Phenotypic characterization of a *Csf1r* haploinsufficient mouse model of adult-onset leukodystrophy with axonal spheroids and pigmented glia (ALSP). *Neurobiol. Dis.* **74**, 219–228 (2015).
13. R. J. Guerreiro, E. Lohmann, J. M. Bras, J. R. Gibbs, J. D. Rohrer, N. Gurunlian, B. Dursun, B. Bilgic, H. Hanagasi, H. Gurvit, M. Emre, A. Singleton, J. Hardy, Using exome sequencing to reveal mutations in TREM2 presenting as a frontotemporal dementia-like syndrome without bone involvement. *JAMA Neurol.* **70**, 78–84 (2013).
14. M. E. Meuwissen, R. Schot, S. Buta, G. Oudesluijs, S. Tinschert, S. D. Speer, Z. Li, L. van Unen, D. Heijsman, T. Goldmann, M. H. Lequin, J. M. Kros, W. Stam, M. Hermann, R. Willemsen, R. W. Brouwer, I. W. F. Van, M. Martin-Fernandez, I. de Coo, J. Dudink, F. A. de Vries, A. B. Avella, M. Prinz, Y. J. Crow, F. W. Verheijen, S. Pellegrini, D. Bogunovic, G. M. Mancini, Human USP18 deficiency underlies type 1 interferonopathy leading to severe pseudo-TORCH syndrome. *J. Exp. Med.* **213**, 1163–1174 (2016).
15. M. T. Heneka, M. P. Kummer, E. Latz, Innate immune activation in neurodegenerative disease. *Nat. Rev. Immunol.* **14**, 463–477 (2014).
16. Y. J. Jung, W. S. Chung, Phagocytic roles of glial cells in healthy and diseased brains. *Biomol. Ther.* **26**, 350–357 (2018).
17. K. Takahashi, C. D. Rochford, H. Neumann, Clearance of apoptotic neurons without inflammation by microglial triggering receptor expressed on myeloid cells-2. *J. Exp. Med.* **201**, 647–657 (2005).
18. D. P. Schafer, E. K. Lehrman, A. G. Kautzman, R. Koyama, A. R. Mardinly, R. Yamasaki, R. M. Ransohoff, M. E. Greenberg, B. A. Barres, B. Stevens, Microglia sculpt postnatal neural circuits in an activity and complement-dependent manner. *Neuron* **74**, 691–705 (2012).
19. L. Weinhard, G. di Bartolomei, G. Bolasco, P. Machado, N. L. Schieber, U. Neniskyte, M. Exiga, A. Vadisiute, A. Raggioli, A. Schertel, Y. Schwab, C. T. Gross, Microglia remodel synapses by presynaptic trogocytosis and spine head filopodia induction. *Nat. Commun.* **9**, 1228 (2018).
20. J. D. Crapser, J. Ochaba, N. Soni, J. C. Reidling, L. M. Thompson, K. N. Green, Microglial depletion prevents extracellular matrix changes and striatal volume reduction in a model of Huntington's disease. *Brain* **143**, 266–288 (2020).
21. P. T. Nguyen, L. C. Dorman, S. Pan, I. D. Vainchtein, R. T. Han, H. Nakao-Inoue, S. E. Taloma, J. J. Barron, A. B. Molofsky, M. A. Kheirbek, A. V. Molofsky, Microglial remodeling of the extracellular matrix promotes synapse plasticity. *Cell* **182**, 388–403.e15 (2020).
22. J. Luo, F. Elwood, M. Britschgi, S. Villeda, H. Zhang, Z. Ding, L. Zhu, H. Alabsi, R. Getachew, R. Narasimhan, R. Wabl, N. Fainberg, M. L. James, G. Wong, J. Relton, S. S. Gambhir, J. W. Pollard, T. Wyss-Coray, Colony-stimulating factor 1 receptor (*CSF1R*) signaling in injured neurons facilitates protection and survival. *J. Exp. Med.* **210**, 157–172 (2013).
23. S. Nandi, S. Gokhan, X. M. Dai, S. Wei, G. Enikolopov, H. Lin, M. F. Mehler, E. R. Stanley, The CSF-1 receptor ligands IL-34 and CSF-1 exhibit distinct developmental brain expression patterns and regulate neural progenitor cell maintenance and maturation. *Dev. Biol.* **367**, 100–113 (2012).
24. N. Oosterhof, I. J. Chang, E. G. Karimiani, L. E. Kuil, D. M. Jensen, R. Daza, E. Young, L. Astle, H. C. van der Linde, G. M. Shivaram, J. Demmers, C. S. Latimer, C. D. Keene, E. Loter, R. Maroofian, T. J. van Ham, R. F. Hevner, J. T. Bennett, Homozygous mutations in *CSF1R* cause a pediatric-onset leukoencephalopathy and can result in congenital absence of microglia. *Am. J. Hum. Genet.* **104**, 936–947 (2019).
25. M. R. Elmore, A. R. Najafi, M. A. Koike, N. N. Dagher, E. E. Spangenberg, R. A. Rice, M. Kitazawa, B. Matusow, H. Nguyen, B. L. West, K. N. Green, Colony-stimulating factor 1 receptor signaling is necessary for microglia viability, unmasking a microglia progenitor cell in the adult brain. *Neuron* **82**, 380–397 (2014).
26. N. Oosterhof, L. E. Kuil, H. C. van der Linde, S. M. Burm, W. Berdowski, W. F. J. van Ijcken, J. C. van Swieten, E. M. Hol, M. H. G. Verheijen, T. J. van Ham, Colony-Stimulating Factor 1 Receptor (*CSF1R*) regulates microglia density and distribution, but not microglia differentiation in vivo. *Cell Rep.* **24**, 1203–1217.e6 (2018).
27. E. Spangenberg, P. L. Severson, L. A. Hohsfield, J. Crapser, J. Zhang, E. A. Burton, Y. Zhang, W. Spevak, J. Lin, N. Y. Phan, G. Habets, A. Rymar, G. Tsang, J. Walters, M. Nespi, P. Singh, S. Broome, P. Ibrahim, C. Zhang, G. Bollag, B. L. West, K. N. Green, Sustained microglial depletion with CSF1R inhibitor impairs parenchymal plaque development in an Alzheimer's disease model. *Nat. Commun.* **10**, 3758 (2019).
28. H. Akiyama, T. Nishimura, H. Kondo, K. Ikeda, Y. Hayashi, P. L. McGeer, Expression of the receptor for macrophage colony stimulating factor by brain microglia and its upregulation in brains of patients with Alzheimer's disease and amyotrophic lateral sclerosis. *Brain Res.* **639**, 171–174 (1994).
29. Y. Wang, O. Berezovska, S. Fedoroff, Expression of colony stimulating factor-1 receptor (CSF-1R) by CNS neurons in mice. *J. Neurosci. Res.* **57**, 616–632 (1999).
30. H. Keren-Shaul, A. Spinrad, A. Weiner, O. Matcovitch-Natan, R. Dvir-Szternfeld, T. K. Ulland, E. David, K. Baruch, D. Lara-Astaiso, B. Toth, S. Itzkovitz, M. Colonna, M. Schwartz, I. Amit, A unique microglia type associated with restricting development of Alzheimer's disease. *Cell* **169**, 1276–1290.e17 (2017).
31. S. Krasemann, C. Madore, R. Cialic, C. Baufeld, N. Calcagno, R. El Fatimy, L. Beckers, E. O'Loughlin, Y. Xu, Z. Fanek, D. J. Greco, S. T. Smith, G. Tweet, Z. Humulock, T. Zrzavy, P. Conde-Sanroman, M. Gacias, Z. Weng, H. Chen, E. Tjon, F. Mazaheri, K. Hartmann, A. Madi, J. D. Ulrich, M. Glatzel, A. Worthmann, J. Heeren, B. Budnik, C. Lemere, T. Ikezu, F. L. Heppner, V. Litvak, D. M. Holtzman, H. Lassmann, H. L. Weiner, J. Ochando, C. Haass, O. Butovsky, The TREM2-APOE pathway drives the transcriptional phenotype of dysfunctional microglia in neurodegenerative diseases. *Immunity* **47**, 566–581.e9 (2017).
32. O. Butovsky, M. P. Jedrychowski, R. Cialic, S. Krasemann, G. Murugaiyan, Z. Fanek, D. J. Greco, P. M. Wu, C. E. Doykan, O. Kiner, R. J. Lawson, M. P. Frosch, N. Pochet, R. E. Fatimy, A. M. Krichevsky, S. P. Gygi, H. Lassmann, J. Berry, M. E. Cudkowicz, H. L. Weiner, Targeting miR-155 restores abnormal microglia and attenuates disease in SOD1 mice. *Ann. Neurol.* **77**, 75–99 (2015).
33. O. Butovsky, M. P. Jedrychowski, C. S. Moore, R. Cialic, A. J. Lanser, G. Gabriely, T. Koeglsperger, B. Dake, P. M. Wu, C. E. Doykan, Z. Fanek, L. Liu, Z. Chen, J. D. Rothstein, R. M. Ransohoff, S. P. Gygi, J. P. Antel, H. L. Weiner, Identification of a unique TGF-β–dependent molecular and functional signature in microglia. *Nat. Neurosci.* **17**, 131–143 (2014).
34. L. Kempthorne, H. Yoon, C. Madore, S. Smith, Z. K. Wszolek, R. Rademakers, J. Kim, O. Butovsky, D. W. Dickson, Loss of homeostatic microglial phenotype in CSF1R-related Leukoencephalopathy. *Acta Neuropathol. Commun.* **8**, 72 (2020).
35. E. P. Azevedo, J. H. Ledo, G. Barbosa, M. Sobrinho, L. Diniz, A. C. Fonseca, F. Gomes, L. Romão, F. R. Lima, F. L. Palhano, S. T. Ferreira, D. Foguel, Activated microglia mediate synapse loss and short-term memory deficits in a mouse model of transthyretin-related oculoleptomeningeal amyloidosis. *Cell Death Dis.* **4**, e789 (2013).
36. R. D. Terry, E. Masliah, D. P. Salmon, N. Butters, R. DeTeresa, R. Hill, L. A. Hansen, R. Katzman, Physical basis of cognitive alterations in Alzheimer's disease: Synapse loss is the major correlate of cognitive impairment. *Ann. Neurol.* **30**, 572–580 (1991).
37. L. A. Glantz, J. H. Gilmore, R. M. Hamer, J. A. Lieberman, L. F. Jarskog, Synaptophysin and postsynaptic density protein 95 in the human prefrontal cortex from mid-gestation into early adulthood. *Neuroscience* **149**, 582–591 (2007).
38. E. C. Onwordi, E. F. Halff, T. Whitehurst, A. Mansur, M. C. Cotel, L. Wells, H. Creeney, D. Bonsall, M. Rogdaki, E. Shatalina, T. Reis Marques, E. A. Rabiner, R. N. Gunn, S. Natesan,

A. C. Vernon, O. D. Howes, Synaptic density marker SV2A is reduced in schizophrenia patients and unaffected by antipsychotics in rats. *Nat. Commun.* **11**, 246 (2020).
39. C. L. Waites, S. A. Leal-Ortiz, N. Okerlund, H. Dalke, A. Fejtova, W. D. Altrock, E. D. Gundelfinger, C. C. Garner, Bassoon and Piccolo maintain synapse integrity by regulating protein ubiquitination and degradation. *EMBO J.* **32**, 954–969 (2013).
40. A. Dityatev, D. A. Rusakov, Molecular signals of plasticity at the tetrapartite synapse. *Curr. Opin. Neurobiol.* **21**, 353–359 (2011).
41. R. Frischknecht, M. Heine, D. Perrais, C. I. Seidenbecher, D. Choquet, E. D. Gundelfinger, Brain extracellular matrix affects AMPA receptor lateral mobility and short-term synaptic plasticity. *Nat. Neurosci.* **12**, 897–904 (2009).
42. T. Pizzorusso, P. Medini, N. Berardi, S. Chierzi, J. W. Fawcett, L. Maffei, Reactivation of ocular dominance plasticity in the adult visual cortex. *Science* **298**, 1248–1251 (2002).
43. H. Tanaka, W. Shan, G. R. Phillips, K. Arndt, O. Bozdagi, L. Shapiro, G. W. Huntley, D. L. Benson, D. R. Colman, Molecular modification of N-cadherin in response to synaptic activity. *Neuron* **25**, 93–107 (2000).
44. J. D. Crapser, E. E. Spangenberg, R. A. Barahona, M. A. Arreola, L. A. Hohsfield, K. N. Green, Microglia facilitate loss of perineuronal nets in the Alzheimer's disease brain. *EBioMedicine* **58**, 102919 (2020).
45. K. A. Giamanco, M. Morawski, R. T. Matthews, Perineuronal net formation and structure in aggrecan knockout mice. *Neuroscience* **170**, 1314–1327 (2010).
46. H. Pantazopoulos, M. Markota, F. Jaquet, D. Ghosh, A. Wallin, A. Santos, B. Caterson, S. Berretta, Aggrecan and chondroitin-6-sulfate abnormalities in schizophrenia and bipolar disorder: A postmortem study on the amygdala. *Transl. Psychiatry* **5**, e496 (2015).
47. N. Hayashi, K. Tatsumi, H. Okuda, M. Yoshikawa, S. Ishizaka, S. Miyata, T. Manabe, A. Wanaka, DACS, novel matrix structure composed of chondroitin sulfate proteoglycan in the brain. *Biochem. Biophys. Res. Commun.* **364**, 410–415 (2007).
48. G. Matuszko, S. Curreli, R. Kaushik, A. Becker, A. Dityatev, Extracellular matrix alterations in the ketamine model of schizophrenia. *Neuroscience* **350**, 13–22 (2017).
49. H. Okuda, K. Tatsumi, S. Morita, Y. Shibukawa, H. Korekane, N. Horii-Hayashi, Y. Wada, N. Taniguchi, A. Wanaka, Chondroitin sulfate proteoglycan tenascin-R regulates glutamate uptake by adult brain astrocytes. *J. Biol. Chem.* **289**, 2620–2631 (2014).
50. M. T. Fitch, J. Silver, Activated macrophages and the blood-brain barrier: inflammation after CNS injury leads to increases in putative inhibitory molecules. *Exp. Neurol.* **148**, 587–603 (1997).
51. V. Chitu, F. Biundo, G. G. L. Shlager, E. S. Park, P. Wang, M. E. Gulinello, S. Gokhan, H. C. Ketchum, K. Saha, M. A. DeTure, D. W. Dickson, Z. K. Wszolek, D. Zheng, A. L. Croxford, B. Becher, D. Sun, M. F. Mehler, E. R. Stanley, Microglial homeostasis requires balanced CSF-1/CSF-2 receptor signaling. *Cell Rep.* **30**, 3004–3019.e5 (2020).
52. N. N. Dagher, A. R. Najafi, K. M. Kayala, M. R. Elmore, T. E. White, R. Medeiros, B. L. West, K. N. Green, Colony-stimulating factor 1 receptor inhibition prevents microglial plaque association and improves cognition in 3xTg-AD mice. *J. Neuroinflammation* **12**, 139 (2015).
53. A. Olmos-Alonso, S. T. Schetters, S. Sri, K. Askew, R. Mancuso, M. Vargas-Caballero, C. Holscher, V. H. Perry, D. Gomez-Nicola, Pharmacological targeting of CSF1R inhibits microglial proliferation and prevents the progression of Alzheimer's-like pathology. *Brain* **139**, 891–907 (2016).
54. D. Gomez-Nicola, N. L. Fransen, S. Suzzi, V. H. Perry, Regulation of microglial proliferation during chronic neurodegeneration. *J. Neurosci.* **33**, 2481–2493 (2013).
55. R. Mancuso, G. Fryatt, M. Cleal, J. Obst, E. Pipi, J. Monzón-Sandoval, E. Ribe, L. Winchester, C. Webber, A. Nevado, T. Jacobs, N. Austin, C. Theunis, K. Grauwen, E. Daniela Ruiz, A. Mudher, M. Vicente-Rodriguez, C. A. Parker, C. Simmons, D. Cash, J. Richardson; NIMA Consortium, D. N. C. Jones, S. Lovestone, D. Gómez-Nicola, V. H. Perry, CSF1R inhibitor JNJ-40346527 attenuates microglial proliferation and neurodegeneration in P301S mice. *Brain* **142**, 3243–3264 (2019).
56. B. M. Davis, M. Salinas-Navarro, M. F. Cordeiro, L. Moons, L. De Groef, Characterizing microglia activation: A spatial statistics approach to maximize information extraction. *Sci. Rep.* **7**, 1576 (2017).
57. M. Nikodemova, R. S. Kimyon, I. De, A. L. Small, L. S. Collier, J. J. Watters, Microglial numbers attain adult levels after undergoing a rapid decrease in cell number in the third postnatal week. *J. Neuroimmunol.* **278**, 280–288 (2015).
58. F. Biundo, V. Chitu, G. G. L. Shlager, E. S. Park, M. E. Gulinello, K. Saha, H. C. Ketchum, C. Fernandes, S. Gökhan, M. F. Mehler, E. R. Stanley, Microglial reduction of colony stimulating factor-1 receptor expression is sufficient to confer adult onset leukodystrophy. *Glia* **69**, 779–791 (2021).
59. E. M. Andrews, R. J. Richards, F. Q. Yin, M. S. Viapiano, L. B. Jakeman, Alterations in chondroitin sulfate proteoglycan expression occur both at and far from the site of spinal contusion injury. *Exp. Neurol.* **235**, 174–187 (2012).
60. Z. W. Li, J. J. Li, L. Wang, J. P. Zhang, J. J. Wu, X. Q. Mao, G. F. Shi, Q. Wang, F. Wang, J. Zou, Epidermal growth factor receptor inhibitor ameliorates excessive astrogliosis and improves the regeneration microenvironment and functional recovery in adult rats following spinal cord injury. *J. Neuroinflammation* **11**, 71 (2014).
61. D. Schulz, Y. Severin, V. R. T. Zanotelli, B. Bodenmiller, In-depth characterization of monocyte-derived macrophages using a mass cytometry-based phagocytosis assay. *Sci. Rep.* **9**, 1925 (2019).
62. C. A. Colton, R. T. Mott, H. Sharpe, Q. Xu, W. E. Van Nostrand, M. P. Vitek, Expression profiles for macrophage alternative activation genes in AD and in mouse models of AD. *J. Neuroinflammation* **3**, 27 (2006).
63. K. N. Green, J. D. Crapser, L. A. Hohsfield, To kill a microglia: A case for CSF1R inhibitors. *Trends Immunol.* **41**, 771–784 (2020).
64. E. C. Warburton, G. R. Barker, M. W. Brown, Investigations into the involvement of NMDA mechanisms in recognition memory. *Neuropharmacology* **74**, 41–47 (2013).
65. T. J. Bussey, J. Duck, J. L. Muir, J. P. Aggleton, Distinct patterns of behavioural impairments resulting from fornix transection or neurotoxic lesions of the perirhinal and postrhinal cortices in the rat. *Behav. Brain Res.* **111**, 187–202 (2000).
66. R. F. Langston, C. H. Stevenson, C. L. Wilson, I. Saunders, E. R. Wood, The role of hippocampal subregions in memory for stimulus associations. *Behav. Brain Res.* **215**, 275–291 (2010).
67. J. W. Fawcett, T. Oohashi, T. Pizzorusso, The roles of perineuronal nets and the perinodal extracellular matrix in neuronal function. *Nat. Rev. Neurosci.* **20**, 451–465 (2019).
68. M. Geissler, C. Gottschling, A. Aguado, U. Rauch, C. H. Wetzel, H. Hatt, A. Faissner, Primary hippocampal neurons, which lack four crucial extracellular matrix molecules, display abnormalities of synaptic structure and function and severe deficits in perineuronal net formation. *J. Neurosci.* **33**, 7742–7755 (2013).
69. C. Gottschling, D. Wegrzyn, B. Denecke, A. Faissner, Elimination of the four extracellular matrix molecules tenascin-C, tenascin-R, brevican and neurocan alters the ratio of excitatory and inhibitory synapses. *Sci. Rep.* **9**, 13939 (2019).
70. M. Blosa, M. Sonntag, C. Jager, S. Weigel, J. Seeger, R. Frischknecht, C. I. Seidenbecher, R. T. Matthews, T. Arendt, R. Rubsamen, M. Morawski, The extracellular matrix molecule brevican is an integral component of the machinery mediating fast synaptic transmission at the calyx of Held. *J. Physiol.* **593**, 4341–4360 (2015).
71. E. Favuzzi, A. Marques-Smith, R. Deogracias, C. M. Winterflood, A. Sánchez-Aguilera, L. Mantoan, P. Maeso, C. Fernandes, H. Ewers, B. Rico, Activity-dependent gating of parvalbumin interneuron function by the perineuronal net protein brevican. *Neuron* **95**, 639–655.e10 (2017).
72. T. S. Balmer, Perineuronal nets enhance the excitability of fast-spiking neurons. *eNeuro* **3**, ENEURO.0112 (2016).
73. J. H. Cabungcal, P. Steullet, H. Morishita, R. Kraftsik, M. Cuenod, T. K. Hensch, K. Q. Do, Perineuronal nets protect fast-spiking interneurons against oxidative stress. *Proc. Natl. Acad. Sci. U.S.A.* **110**, 9130–9135 (2013).
74. N. Hagan, J. L. Kane, D. Grover, L. Woodworth, C. Madore, J. Saleh, J. Sancho, J. Liu, Y. Li, J. Proto, M. Zelic, A. Mahan, M. Kothe, A. A. Scholte, M. Fitzgerald, B. Gisevius, A. Haghikia, O. Butovsky, D. Ofengeim, CSF1R signaling is a regulator of pathogenesis in progressive MS. *Cell Death Dis.* **11**, 904 (2020).
75. J. C. Nissen, K. K. Thompson, B. L. West, S. E. Tsirka, Csf1R inhibition attenuates experimental autoimmune encephalomyelitis and promotes recovery. *Exp. Neurol.* **307**, 24–36 (2018).
76. D. A. Hume, M. Caruso, M. Ferrari-Cestari, K. M. Summers, C. Pridans, K. M. Irvine, Phenotypic impacts of CSF1R deficiencies in humans and model organisms. *J. Leukoc. Biol.* **107**, 205–219 (2020).
77. C. Pridans, K. A. Sauter, K. Baer, H. Kissel, D. A. Hume, CSF1R mutations in hereditary diffuse leukoencephalopathy with spheroids are loss of function. *Sci. Rep.* **3**, 3013 (2013).
78. W. T. Tian, F. X. Zhan, Q. Liu, X. H. Luan, C. Zhang, L. Shang, B. Y. Zhang, S. J. Pan, F. Miao, J. Hu, P. Zhong, S. H. Liu, Z. Y. Zhu, H. Y. Zhou, S. Sun, X. L. Liu, X. J. Huang, J. W. Jiang, J. F. Ma, Y. Wang, S. F. Chen, H. D. Tang, S. D. Chen, L. Cao, Clinicopathologic characterization and abnormal autophagy of CSF1R-related leukoencephalopathy. *Transl. Neurodegener.* **8**, 32 (2019).
79. E. J. Kim, J. H. Shin, J. H. Lee, J. H. Kim, D. L. Na, Y. L. Suh, S. J. Hwang, J. H. Lee, Y. M. Lee, M. J. Shin, M. J. Lee, S. J. Kim, U. Yoon, D. Y. Park, D. S. Jung, J. W. Ahn, S. Sung, G. Y. Huh, Adult-onset leukoencephalopathy with axonal spheroids and pigmented glia linked CSF1R mutation: Report of four Korean cases. *J. Neurol. Sci.* **349**, 232–238 (2015).
80. C. Wang, H. Yue, Z. Hu, Y. Shen, J. Ma, J. Li, X. D. Wang, L. Wang, B. Sun, P. Shi, L. Wang, Y. Gu, Microglia mediate forgetting via complement-dependent synaptic elimination. *Science* **367**, 688–694 (2020).
81. R. Rojo, A. Raper, D. D. Ozdemir, L. Lefevre, K. Grabert, E. Wollscheid-Lengeling, B. Bradford, M. Caruso, I. Gazova, A. Sánchez, Z. M. Lisowski, J. Alves, I. Molina-Gonzalez, H. Davtyan, R. J. Lodge, J. D. Glover, R. Wallace, D. A. D. Munro, E. David, I. Amit, V. E. Miron, J. Priller, S. J. Jenkins, G. E. Hardingham, M. Blurton-Jones, N. A. Mabbott, K. M. Summers, P. Hohenstein, D. A. Hume, C. Pridans, Deletion of a *Csf1r* enhancer selectively impacts CSF1R expression and development of tissue macrophage populations. *Nat. Commun.* **10**, 3215 (2019).

82. C. Pridans, A. Raper, G. M. Davis, J. Alves, K. A. Sauter, L. Lefevre, T. Regan, S. Meek, L. Sutherland, A. J. Thomson, S. Clohisey, S. J. Bush, R. Rojo, Z. M. Lisowski, R. Wallace, K. Grabert, K. R. Upton, Y. T. Tsai, D. Brown, L. B. Smith, K. M. Summers, N. A. Mabbott, P. Piccardo, M. T. Cheeseman, T. Burdon, D. A. Hume, Pleiotropic impacts of macrophage and microglial deficiency on development in rats with targeted mutation of the *Csf1r* locus. *J. Immunol.* **201**, 2683–2699 (2018).
83. J. Li, K. Chen, L. Zhu, J. W. Pollard, Conditional deletion of the colony stimulating factor-1 receptor (c-fms proto-oncogene) in mice. *Genesis* **44**, 328–335 (2006).
84. M. R. P. Elmore, L. A. Hohsfield, E. A. Kramar, L. Soreq, R. J. Lee, S. T. Pham, A. R. Najafi, E. E. Spangenberg, M. A. Wood, B. L. West, K. N. Green, Replacement of microglia in the aged brain reverses cognitive, synaptic, and neuronal deficits in mice. *Aging Cell* **17**, e12832 (2018).
85. A. Dobin, C. A. Davis, F. Schlesinger, J. Drenkow, C. Zaleski, S. Jha, P. Batut, M. Chaisson, T. R. Gingeras, STAR: Ultrafast universal RNA-seq aligner. *Bioinformatics* **29**, 15–21 (2013).
86. Y. Liao, G. K. Smyth, W. Shi, The Subread aligner: Fast, accurate and scalable read mapping by seed-and-vote. *Nucleic Acids Res.* **41**, e108 (2013).
87. R Core Team, *R: A Language and Environment for Statistical Computing* (R Foundation for Statistical Computing, 2017).
88. M. D. Robinson, D. J. McCarthy, G. K. Smyth, edgeR: A Bioconductor package for differential expression analysis of digital gene expression data. *Bioinformatics* **26**, 139–140 (2010).
89. B. Zhang, S. Horvath, A general framework for weighted gene co-expression network analysis. *Stat. Appl. Genet. Mol. Biol.* **4**, Article17 (2005).
90. M. V. Kuleshov, M. R. Jones, A. D. Rouillard, N. F. Fernandez, Q. Duan, Z. Wang, S. Koplev, S. L. Jenkins, K. M. Jagodnik, A. Lachmann, M. G. McDermott, C. D. Monteiro, G. W. Gundersen, A. Ma'ayan, Enrichr: A comprehensive gene set enrichment analysis web server 2016 update. *Nucleic Acids Res.* **44**, W90–W97 (2016).

Acknowledgments: We thank B. L. West and A. Rymar at Plexxikon Inc. for providing and formulating CSF1R inhibitor chow. We also thank K. Cramer for providing CSF1R$^{+/-}$ mice to start our colony. **Funding:** This work was supported by the NIH under the following awards: R01NS083801 (NINDS), R01AG056768 (NIA), and U54 AG054349 [NIA Model Organism Development and Evaluation for Late-onset Alzheimer's Disease (MODEL-AD)] to K.N.G.; 1F31NS111882-01A1 (NINDS) to M.A.A.; F31NS108611 (NINDS) to J.D.C.; and AARF-16-442762 (Alzheimer's Association) to L.A.H. The content is solely the responsibility of the authors and does not necessarily represent the official views of the NIH. Sources of funding did not have any role in study design, data collection or analysis, interpretation of results, or manuscript preparation or submission. **Author contributions:** M.A.A. conceived and performed experiments, analyzed data, and wrote the manuscript. N.S. performed experiments. J.D.C. conceived experiments and edited the manuscript. L.A.H. edited the manuscript and provided feedback. M.R.P.E. performed experiments and edited the manuscript. D.P.M. performed experiments. M.A.W., V.S., and A.M. provided guidance in project conceptualization. K.N.G. conceived the experiments, wrote and edited the manuscript, provided supervision, and secured funding. **Competing interests:** K.N.G. sits on the scientific advisory board of Ashvattha Therapeutics. **Data and materials availability:** All data needed to evaluate the conclusions in the paper are present in the paper and/or the Supplementary Materials.

Submitted 15 December 2020
Accepted 2 July 2021
Published 25 August 2021
10.1126/sciadv.abg1601

Citation: M. A. Arreola, N. Soni, J. D. Crapser, L. A. Hohsfield, M. R. P. Elmore, D. P. Matheos, M. A. Wood, V. Swarup, A. Mortazavi, K. N. Green, Microglial dyshomeostasis drives perineuronal net and synaptic loss in a CSF1R$^{+/-}$ mouse model of ALSP, which can be rescued via CSF1R inhibitors. *Sci. Adv.* **7**, eabg1601 (2021).